Observational study of the monsoonal dynamics and eddy shedding phenomena

by

Jelena M. Popovic

B.S., University of Belgrade (1994)

Submitted to the Department of Earth, Atmospheric and Planetary Sciences
in partial fulfillment of the requirements for the degree of

Master of Science

at the

MASSACHUSETTS INSTITUTE OF TECHNOLOGY

May 1999 [June, 1999]

Author .....
Department of Earth, Atmospheric and Planetary Sciences
May 17, 1999

Certified by .....
R. Alan Plumb
Professor of Meteorology
Thesis Supervisor

Accepted by .....
Ronald G. Prinn
Chairman, Department of Earth, Atmospheric and Planetary Sciences

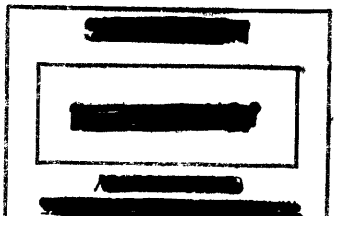

Observational study of the monsoonal dynamics and eddy shedding phenomena

by

Jelena M. Popovic

Submitted to the Department of Earth, Atmospheric and Planetary Sciences
on May 17, 1999, in partial fulfillment of the
requirements for the degree of
Master of Science

Abstract

We analyze atmospheric data in order to study the upper tropospheric dynamics in the area of the Asian summer monsoon. We look at summers of four years from 1987 to 1990.

The divergent upper tropospheric circulation of the monsoon often adopts the form of a unified large-scale vortex. However, when the vortex becomes elongated enough, so that the flow in most of the area is close to zonal, the vortex usually sheds secondary, or daughter, vortices that then propagate away. Eddy shedding occurs in all four summers that we examined.

We use the potential vorticity and Montgomery streamfunction fields to document the characteristics of eddy shedding events. In most cases, the daughter cell propagates westward. In the vertical, eddy shedding is confined to the upper troposphere, between 300 and 100 mb. The relationship between lower convergent and upper divergent levels is strong. However, we have not found any simple relationship between eddy shedding and lower-level dynamics.

Thesis Supervisor: R. Alan Plumb
Title: Professor of Meteorology

Acknowledgments

First, I would like to thank my advisor, Prof. R. Alan Plumb, for supporting me and encouraging me to work independently. I am thankful to him for providing me with the opportunity to work on this interesting topic at a crucial point in my studies. I thank my former advisor, Prof. John Marshall, for taking me on as a student and for his overwhelming enthusiasm.

During three years of my graduate studies at MIT, I enjoyed working in the friendly atmosphere at EAPS department. There are a number of people who helped make my studies pleasant and, when it was necessary, "possible to survive". I am thankful to all of them. Here, I mention just a few individually. My classmates Pablo Zurita, Tieh-Yong Koh, and Caixia Wang were always there for me to discuss the topics related to our classes and research. My devoted friend Caixia, shared with me all the good and bad moments that we encountered during our studies. Francois Primeau gave me much scientific advice at the beginning of my studies and research here. Natalia Beliakova was a great friend, full of useful advice and optimism. The results of Juno Hsu's thesis were an important motivating factor for the research presented in this thesis. I am thankful for her advice and encouragement to continue in this direction. Rebecca Morss and Constantine Giannitsis helped greatly with their comments and suggestions on the first drafts of this thesis. I am indebted to Vince Larson, who helped a great deal in the proofreading of the final version of this thesis.

Thanks to Linda Meinke for maintaining the computer networks on all three floors where I worked. Stacey Frangos helped answer all possible questions about the administrative aspects of graduate school since the time when I was still in Belgrade applying for graduates studies here.

Finally, I am grateful to my family. I dedicate this thesis to my parents Mirjana and Marko Popovic. Their love, support, and encouragement has benefited me without measure. I am indebted to my grandmother Ana Popovic for her wisdom and love. Thanks to Djordje Popovic for being the best brother in the world. In the five years since I met Marko Popovic (Junior), he has been a tremendous source of love and companionship. I thank him for bearing and sharing all things with me, positive and negative, big and small. Without his help and encouragement I would not have been able to finish this thesis.

Contents

List of Figures

Chapter 1

Introduction

1.1 Monsoon dynamics

Monsoonal circulations are found over tropical regions of Asia, Australia, Africa and to some extent North America. A circulation is considered monsoonal if the wind reverses direction between summer and winter. In summer, monsoons are characterized by intense precipitation. The accumulated rainfall in monsoonal areas is generally much higher than in other parts of the world. The important driver of monsoonal circulation is the land-sea contrast, i.e. the different thermal characteristics of land and sea surfaces. Therefore, monsoons are found where a continent borders an ocean, and where wind blows inland from the cooler oceans toward the warm continents in summer, and from the cold continents toward the warm oceans in winter.

Figures 1-1 and 1-2 show the precipitation and lower level winds (850 mb), for July and January of 1987–1990. In northern summer, enhanced precipitation is found in central America, western tropical Africa, and southern Asia. In southern summer, enhanced precipitation is found in tropical South America, in southern tropical Africa, and in Indonesia and northern Australia. The African monsoon seems to be the weakest in terms of precipitation, but a wind reversal is present there. Intense rainfall in the tropical area of the American continent suggests a monsoonal circulation. However, a wind reversal is not seen there. The best example of monsoonal circulation is found in the Asian-Australian area. Here we see both a drastic wind reversal and extremely abundant rainfall.

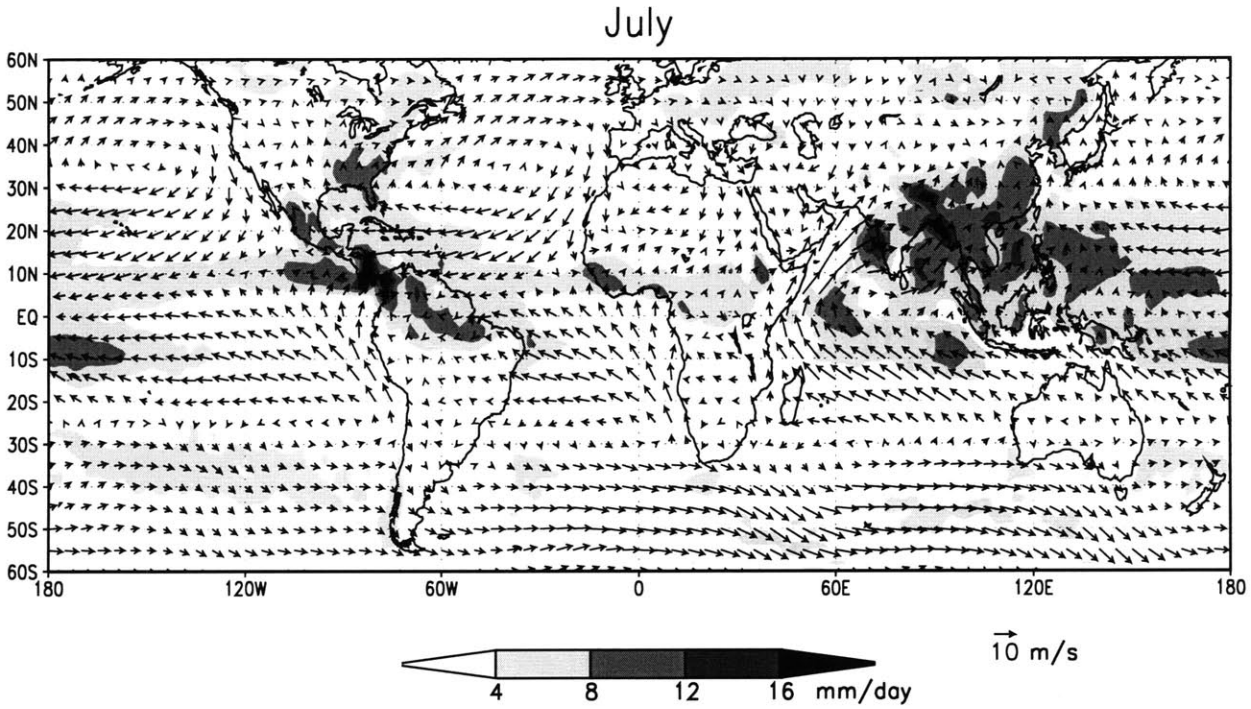

Figure 1-1: July 1987-90 mean precipitation rate and wind vectors at 850 mb.

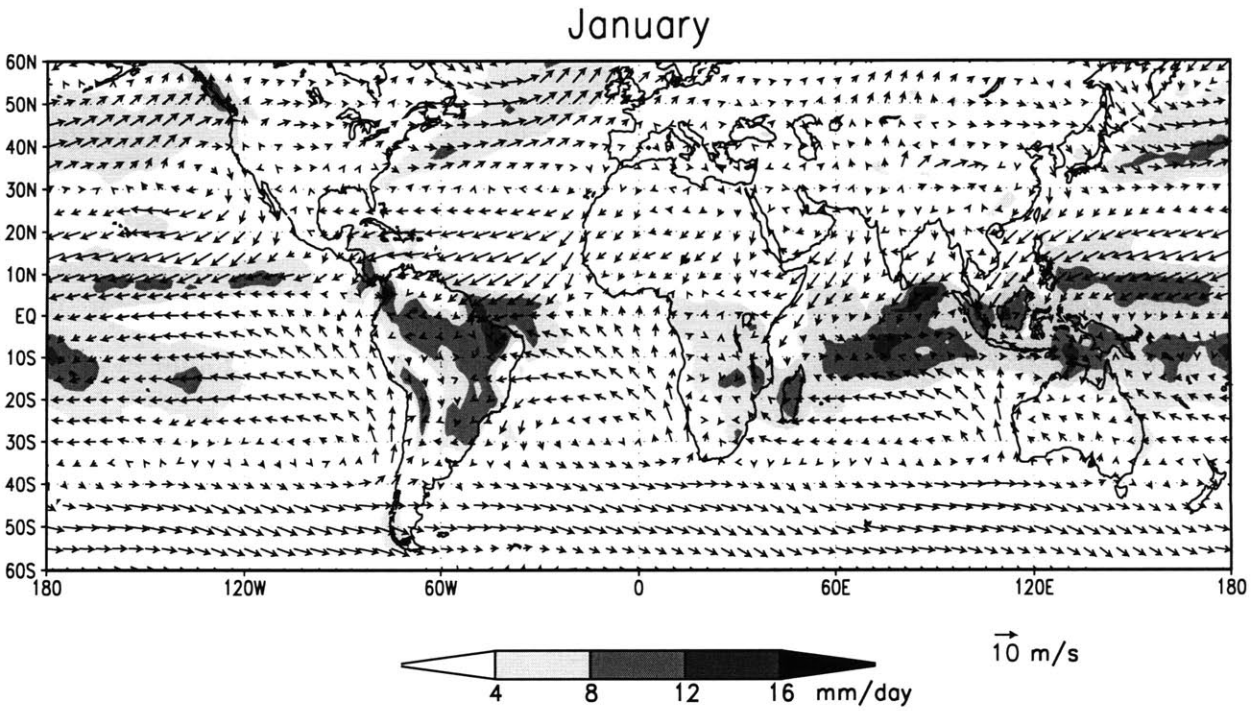

Figure 1-2: January 1987-90 mean precipitation rate and wind vectors at 850 mb.

The Asian summer monsoon alone is so strong that it appears to be one of the main contributors to the zonally averaged fields of the Hadley cell. The reason for such a strong monsoonal circulation, beside the strong land-sea contrast, is the presence of the characteristic topographic feature in this region - the Tibetan plateau. This massive feature, with average height of 4000 m, influences the monsoonal circulation by acting as an additional heat source as well as a mechanical barrier for the winds.

During the Asian summer monsoon, the lower troposphere is characterized by strong cross-equatorial flow (Figure 1-1). Southwesterly flow, off the Eastern African coast and over the Arabian Sea, brings moisture to the Indian subcontinent. Warming of the continent and near-surface air results in strong convection, and hence latent heat release. This latent heating, enhanced by sensible heating from the Tibetan plateau, helps warm the whole troposphere in this area. The low-level convergence and ascending motion in this area of strong convection are associated with the strong divergent flow in the upper troposphere. Large scale anticyclonic circulation is seen in the area of the Asian summer monsoon during the whole summer.

The Asian summer monsoon lasts for four months. The onset of the monsoon, which is marked by a sudden change of wind direction and a spectacular onset of rainfall, is usually very rapid. The onset of the monsoon over southern tip of the Indian subcontinent normally occurs between May 25 and June 1. Then the monsoon gradually progresses onto land. It is normally established over the entire Indian subcontinent by July 1.

During the established phase, the monsoon exhibits substantial variability. Monsoon depressions are synoptic systems, of roughly a few days duration, which occur several times during the established phase. These are accompanied by a large amount of rainfall. The active/break cycle happens on time scales of one to two weeks. Active and break monsoon spells exhibit contrasting features with respect to rainfall and flow patterns (Desai 1987, Das 1987). These phases of the monsoon are associated with the intensity and position of the monsoon trough. The monsoon trough represents the zone of low pressure over the plains of northern India. The axis of this trough is normally oriented in a northwest-southeast direction and it normally extends up to the 500 mb level, tilting southwards with height. The active phase of the monsoon occurs when the trough axis is to the south of its normal

position with one or two cyclonic vortices embedded in it. It is characterized by a large amount of well-distributed rainfall over the plains of Northern India, the central parts of the country, and along the west coast. The break in monsoon activity happens when the trough axis moves to the north and lies close to the Himalayas. In this phase, the heavy and well-distributed rainfall is only found along the foothills of the Himalayas, northeast India, and southeast Peninsular India.

The retreat of the monsoon starts around September 1 in the northwestern parts of India. The monsoon normally withdraws from northern and central India by October 15.

The amount of rainfall received during the summer monsoonal season as well as its timing clearly establish the great importance and need (economic and otherwise) for better understanding of monsoonal dynamics. Intensive interest is especially expressed in India and other countries directly influenced by monsoons. Because of this, the published literature on the theory and prediction of monsoons is extensive. However, the role and importance of the Asian summer monsoon, although greatest in the areas of abundant rainfall, is not limited only to these regions. It is also part of the global scale circulation in the tropics, and it is important to understand it in this broader aspect as well (recent literature includes Hoskins and Rodwell 1995, Sardeshmukh and Held 1984).

This thesis focuses mainly on the large scale upper tropospheric divergent circulation in the area of the Asian summer monsoon and the eddy shedding phenomenon which is found to appear in this region. The relation between this upper tropospheric phenomenon and dynamics of the lower tropospheric levels is addressed as well.

1.2 Theoretical aspects of eddy shedding

The dynamically interesting phenomenon of "eddy shedding", found both in numerical experiments and observations (Hsu, 1998), inspired this work. The term "eddy shedding" implies the existence of a "mother" vortex from which secondary (or "daughter") vortices detach (shed) and propagate away. In the numerical model of Hsu (1998), for certain ranges of parameters, eddy shedding occurs periodically, and a daughter vortex is seen to propagate either westward or eastward depending on the type of the asymmetry imposed. Looking at

atmospheric data and concentrating on the month of July 1990, Hsu (1998) found two eddy shedding events in the monsoonal anticyclone, characterized by westward propagation of the secondary vortex. However, does eddy shedding happen every summer? How often does it happen? Is there any periodicity in eddy shedding occurrence? What are the circumstances responsible for its occurrence? What are its time and space scales? How does this upper tropospheric phenomenon interact with the lower level dynamics of the monsoon? To address these and similar questions we analyze atmospheric data and present the results of our analysis in Chapter 3.

The current theoretical understanding of eddy shedding dynamics developed to some extent along the line of the studies related to Hadley cell dynamics. The Hadley cell, an important part of the general circulation of the atmosphere has been successfully modeled using simple balances for angular momentum and thermal energy. One of the first in a series of papers dealing with the Hadley circulation was by Held and Hou (1980). They considered the axially symmetric circulation forced by the annually averaged thermal forcing centered on the equator. For a (nearly) inviscid atmosphere they obtained a solution with two overturning cells symmetric around the Equator and confined to the region of the angular momentum conservation (AMC). Outside that region, the solution was in thermal equilibrium (TE). In a following paper by Lindzen and Hou (1988), a more realistic solution was obtained by applying a thermal forcing centered off the Equator. They obtained one strong (winter) Hadley cell and a weak secondary cell in the summer hemisphere, similar to what one sees by looking at the zonally averaged observational data.

The interesting conversion from the spherical geometry and axially symmetric solutions of Held and Hou (1980) (the axis of symmetry being the Earth's axis of rotation) to the f plane geometry with axially symmetric thermal forcing (the axis of symmetry being vertical axis in the center of the domain) was performed by Hsu and Plumb (1998).

Hsu and Plumb (1998) derived the equivalent of Held and Hou's solution in a shallow-water model on an f plane, consisting of AMC and TE solutions matched at a location which is determined by requiring that no mass is lost within the region that the angular momentum solution holds. The model simulates the thermally driven nonlinear, inviscid, divergent circulation. The thermal forcing is included through the mass relaxation and is

locally axisymmetric. The goal of their study was to look at the behavior of the circulation when non-axisymmetric elements are applied to the steady state axisymmetric circulation.

In Hsu and Plumb, the asymmetries were imposed in the problem in two ways - by including a uniform zonal flow (uniform flow experiments) or by adding the β effect, i.e. adding the planetary vorticity gradient (β plane experiments). The control parameters for the runs are expressed as the ratio of the velocity induced by the asymmetric element to the magnitude of the localized divergent flow induced by the axisymmetric thermal forcing. If the control parameter is smaller than some critical value, the model flow is in a "subcritical" regime: the central vortex remains united but with the center shifted south-eastward (in the uniform flow experiments) or south-westward (in the β plane experiments). For the larger values of the control parameters, the model flow is in a "supercritical" regime: the vortex structure is distorted such that the main anticyclone periodically sheds eddies eastward (in the uniform flow experiments) or westward (in the β plane experiments).

The model in Hsu and Plumb may correspond to the flow in the upper troposphere in the Asian summer monsoon because the flow in this area is anticyclonic, i.e. divergent. In addition, studies of the vorticity budget show that the vorticity balance is essentially nonlinear and nearly inviscid in this area (Sardeshmukh and Held 1984, Sardeshmukh and Hoskins 1985). The primary balance is between the divergence term and advection of absolute vorticity by the time mean horizontal flow. These conclusions are drawn from the vorticity budget derived both from the ECMWF (European Center for Medium Range Forecast) data analysis (Sardeshmukh and Hoskins 1985) and from a general circulation model (Sardeshmukh and Held 1984) which produces a reasonable simulation of the large-scale features of the northern summer tropical upper tropospheric flow without the inclusion of sub-grid scale processes that strongly damp the upper tropospheric vorticity.

1.3 Outline

The upper tropospheric dynamics in the area of the Asian summer monsoon is the main focus of this observational study. We analyzed summers of 1987 to 1990, looking for the evidence of eddy shedding, previously found by Hsu and Plumb (1998) for summer 1990.

Chapter 2 contains the description of data used in the study. Chapter 3 presents the results of the observational study. It starts with a presentation of the summer climatology. This is followed by a sample case of eddy shedding from July 1990. The main characteristics of the upper tropospheric circulation in the Asian monsoonal region, and other eddy shedding events, are presented next. At the end of Chapter 3, the relation to the lower tropospheric dynamics is discussed. Chapter 4 summarizes the most important conclusions of this thesis.

Chapter 2

Data

2.1 NCAR/NCEP Reanalysis

The data used in this study are the NCEP/NCAR (National Center for Environmental Prediction/National Center for Atmospheric Research) Reanalysis data. This data set is global with horizontal resolution 2.5° latitude by 2.5° longitude (73 by 144 grid points). There are 17 standard pressure levels used: 1000, 925, 850, 700, 600, 500, 400, 300, 250, 200, 150, 100, 70, 50, 30, 20, and 10 mb. Data output is available every 6 hours at 0000, 0600, 1200 and 1800 UTC. We use pressure level data of zonal and meridional wind components (u and v), air temperature (T), and geopotential height (h), from 1987 to 1990. The NCEP/NCAR reanalysis also provides data of relative and specific humidity and the vertical velocity component (ω) at 8 lower levels from 1000 to 300 mb. These data are available on the tapes stored in netCDF files.

Other fields that are available at this same horizontal resolution include surface data and data at the tropopause level (temperature and pressure). Set of data including fluxes, precipitation, clouds, and similar are given on a Gaussian grid, with a resolution of 94 by 192 grid points. From this set of data we looked at the precipitation rate. Daily means of these data fields are available to us from the NCEP/NCAR web page.

The main point of the reanalysis project is to have a unified way of constructing a gridded data set throughout a long period of time. Therefore, in the NCEP/NCAR Reanalysis, a frozen state-of-the-art analysis/forecast system was used to perform data assimilation using

the past data from 1957 to 1997 (Kalnay et al., 1996). The same frozen analysis/forecast system continued to be used from 1997 to the present. The observing system has been changing with time (since 1957). The Reanalysis project makes use of the most data available at any time.

In the Tropics, one of the greatest improvements of analyses and forecasts was made by the replacement of OI (optimal interpolation) analysis by SSI (spectral statistical interpolation) analysis (Kalnay et al. 1996). Variables that were most sensitive to the changes in the analysis-forecast system were upper-level divergent flow, precipitation, and stratospheric winds.

In general, there are four categories of data in the Reanalysis, depending on how much information comes directly from the observations and how much is determined from the model. The most reliable class of data (class A), in which the analysis variable is strongly influenced by observed data, includes temperature, wind and geopotential height. Class B consists of those analysis variables whose values are directly affected by the observational data, but which are also strongly influenced by the model. Some examples are humidity, vertical velocity, surface temperature. The diagnostic fields mostly fall into class C: no observations directly affect the variable, and the values are determined solely from the model fields, forced by the data assimilation to remain close to the atmosphere (e. g. precipitation, clouds, surface fluxes). And the forth class D represents fields which are obtained from climatological values and which do not depend on the model (e.g. surface roughness, land-sea mask).

2.2 Data set from 1987 to 1990

In the set of four years that we analyzed, Asian summer monsoon rainfall was below normal in 1987 and above normal in 1988 to 1990. The contrast in the amount of monsoonal rainfall between 1987 and 1988 was studied by a number of authors (e.g. Krishnamurti 1989, 1990, Inoue 1997, Kalnay et al. 1996, Schaack and Johnson 1994). In some of these studies, the relation between the El Nino-Southern Oscillation (ENSO) "state" and the amount of the monsoonal rainfall is drawn. This is because 1987 was a warm ENSO episode (El Nino) and

1988 was a cold ENSO episode (La Nina). However, although weak monsoons (monsoons with sub-normal rainfall) are frequently associated with El Nino, the correspondence between the strength of the rainfall anomaly and the strength of El Nino is not always strong (Slingo 1997).

Chapter 3

Results of data analysis

3.1 Isentropic coordinates and the time mean fields

For the visualization of the dynamics of the upper tropospheric monsoon circulation, we will mainly use isentropic (or θ) coordinates. This vertical coordinate is chosen because it offers the best way of representing Ertel's potential vorticity (P). "PV-thinking," in turn, is a powerful way of viewing dynamics (Hoskins et al. 1985). Ertel's potential vorticity is in general defined as $P = \rho^{-1}\zeta_a \cdot \nabla\theta$, where ρ is density, ζ_a is the absolute vorticity and θ is potential temperature (Andrews et al. 1987). In adiabatic, frictionless flow Ertel's potential vorticity is conserved following the motion. Therefore, it represents an excellent tracer for motions on time scales smaller than the time scales for friction and diabatic heating. Potential vorticity is very useful in one more sense. Once the potential vorticity field is known, we can use the invertibility principle to calculate the streamfunction. Thence, we are able to deduce the wind, pressure and temperature fields.

The NCEP/NCAR data are given on pressure levels. In order to work in isentropic coordinates, we had to interpolate the data to isentropic surfaces. Specifically, we first calculated potential temperature θ on pressure levels, then calculated the pressure for desired isentropic surfaces, and finally linearly interpolated all the needed variables onto those isentropic surfaces.

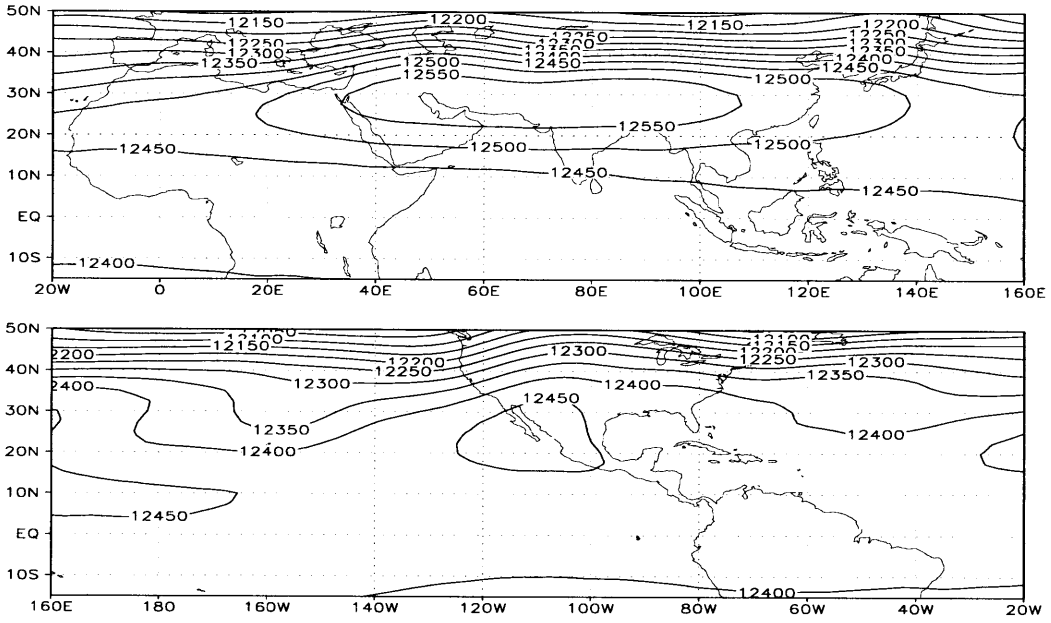

Figure 3-1: July 1987-90 mean geopotential height field at 200 mb.

Potential vorticity in isentropic spherical coordinates is given by

$$P = \frac{\zeta_{a\theta}}{\sigma} \tag{3.1}$$

where

$$\sigma = -\frac{1}{g}\frac{\partial p}{\partial \theta} \tag{3.2}$$

is the effective "density" and

$$\zeta_{a\theta} = \frac{1}{a\cos\phi}\frac{\partial v}{\partial \lambda} - \frac{1}{a}\frac{\partial u}{\partial \phi} + \frac{u\tan\phi}{a} + f \tag{3.3}$$

is the vertical component of absolute isentropic vorticity. The other symbols have their usual meaning: g is gravitational acceleration, p is pressure, u and v are the horizontal components of the wind, a is the radius of the Earth, and ϕ and λ represent the latitude and longitude of the Earth.

Let us first look at the main characteristics of the upper tropospheric summer monsoon

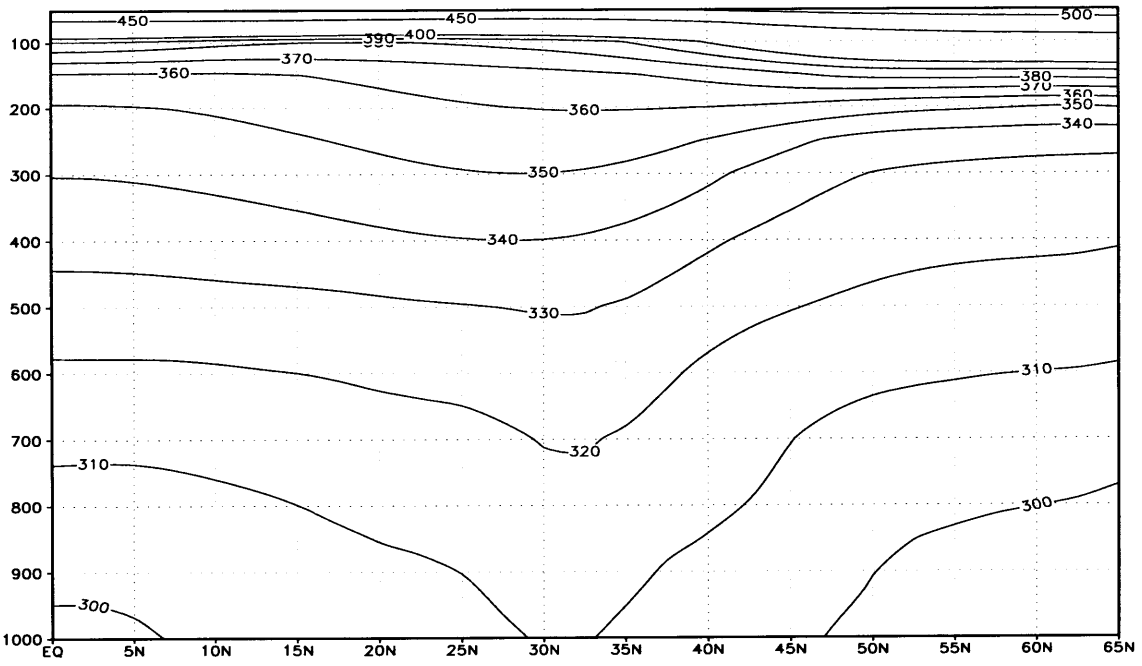

Figure 3-2: July 1987-90 mean potential temperature zonally averaged from 40°E to 100°E.

circulation. In this study, we analyzed four years of data, from 1987 to 1990. July monthly mean fields averaged over these four years are assumed to represent the July (summer) climatology. The dominant feature of the 200 mb (upper troposphere) geopotential height field is anticyclonic circulation centered over south Asia and extending over almost half of the globe (Figure 3-1).

The large scale zonal asymmetry in the summer global mean circulation in the Asian monsoon region is caused by diabatic heating associated with the monsoon. One of the principal heat sources during northern summer is located in the region of the Asian summer monsoon. The maximum heating exceeds 300 W m^{-2} over the northern Bay of Bengal (Yanai and Tomita 1998). From the analysis of the horizontal and vertical profiles of the heat sources and moisture sinks, Yanai and Tomita showed that the major component of the heat source during northern summer in the tropics is latent heat released by cumulus convection. Over land areas at higher latitudes, including the Tibetan Plateau, their analysis implies that sensible heating from the ground is also significant.

For our area of interest ($\sim$ 30°N), the isentropic surfaces that correspond to the upper

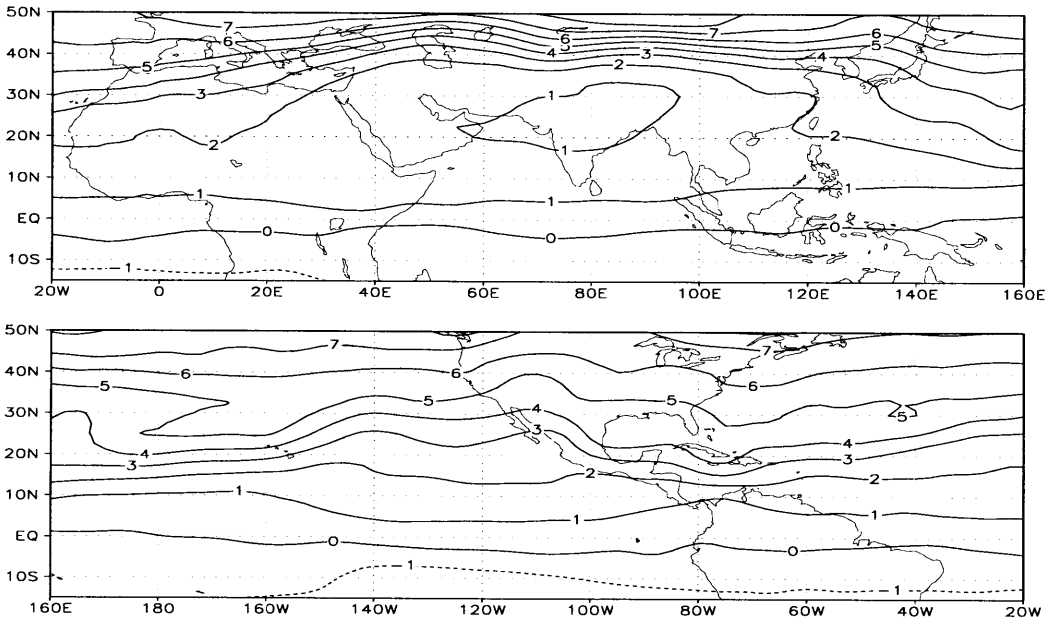

Figure 3-3: July 1987-90 mean IPV field at 370 K.

troposphere (between roughly 300 and 100 mb) are 350 K to 390 K. This may be seen from Figure 3-2, where the time mean θ field for July is zonally averaged between 40°E and 100°E. Therefore, we chose the 370 K isentropic surface as the representative isentropic level of the upper troposphere dynamics for most of the figures that follow.

The mean July isentropic potential vorticity (IPV) field at 370 K is shown in Figure 3-3. Potential vorticity is given in PV units where 1 PVU = 10^{-6} K kg^{-1} m^2 s^{-1}. Tropospheric values of PV are generally below about 1.5 PVU. Typically, there is a sharp jump of PV at the tropopause to stratospheric values of about 4 PVU, and there is a further steep rise of PV with height in the stratosphere. From Figure 3-3 we see that the upper tropospheric anticyclone is characterized by low PV, considerably lower than at other places at the same latitude on this isentropic surface. Elsewhere, such low PV values are found only within a few degrees of the equator. This can be viewed as a signature of the recurrent convective heating below.

Since we are analyzing the PV field on isentropic surfaces, it is convenient to interpolate the wind to those surfaces, as well. Figure 3-4 displays the July mean wind field at 370 K in

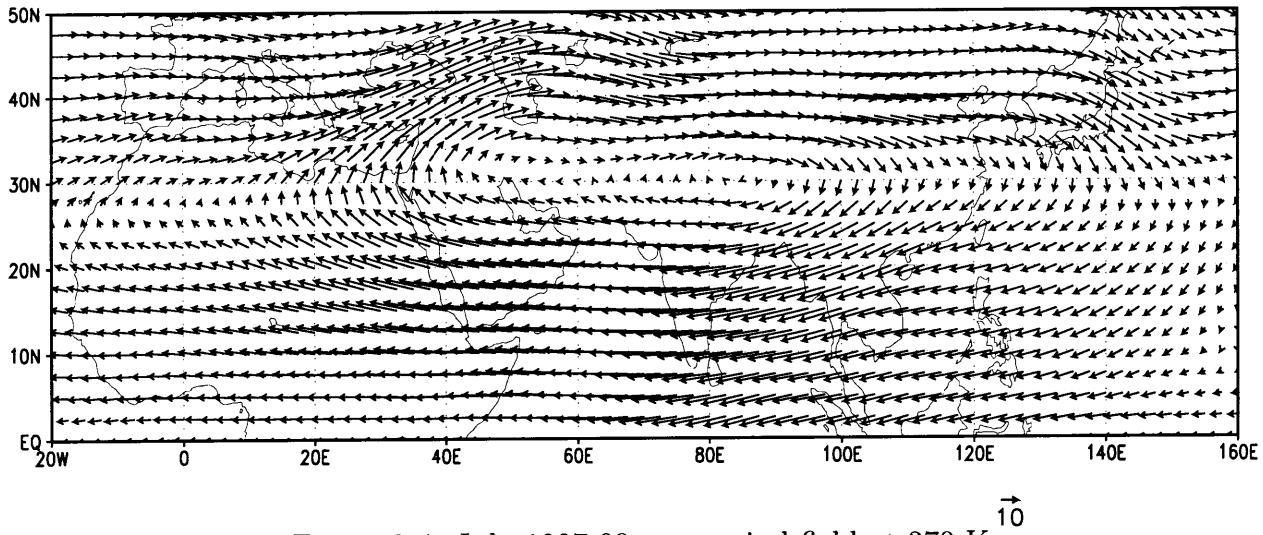

Figure 3-4: July 1987-90 mean wind field at 370 K.

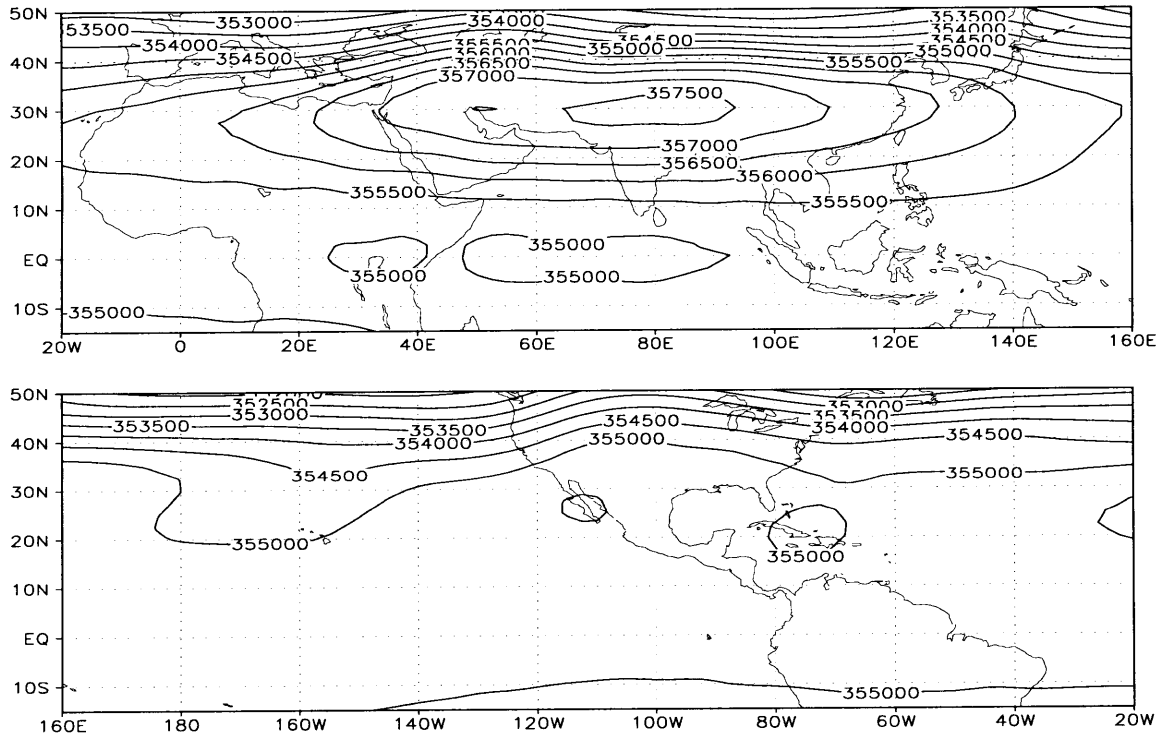

Figure 3-5: July 1987-90 mean Montgomery streamfunction field at 370 K.

the area of the anticyclone. The Montgomery streamfunction (M) is another variable which is natural to use in the isentropic coordinate system. The transformation of the horizontal pressure gradient force from z to θ coordinates is given by $\frac{1}{\rho}\nabla_z p = \nabla_\theta M$. Therefore, in the geostrophic balance in θ coordinates, wind vectors are parallel to the isolines of M. The Montgomery streamfunction is defined by

$$M = c_p T + \Phi \tag{3.4}$$

where c_p=1004 J kg^{-1} K^{-1} is the specific heat at constant pressure, T is temperature, and $\Phi = gz$ is the geopotential. Mean July Montgomery streamfunction field at 370 K in units of m^2 s^{-2} is presented in Figure 3-5. Similar to the geopotential height field (Figure 3-1), the Montgomery streamfunction field is characterized by mid-Pacific and mid-Atlantic troughs, and most dominantly by the large scale anticyclonic circulation in the eastern half of the globe. In what follows we analyze the characteristics of this anticyclonic circulation in more detail.

3.2 Eddy shedding in the atmospheric data

In this and the following section we show evidence of eddy shedding in the atmosphere and explain why it may occur. In July of four analyzed years, eddy shedding occurred several times. In this section we present the event in July 1990, which appears to be the "cleanest" case in these four years.

Before we look at the time evolution of the fields in the upper troposphere, we present the monthly mean IPV fields at 370 K for winter and summer months of years 1987-90, thus contrasting these two different seasonal regimes (Figure 3-6). In this and other color figures that follow, the IPV on the 370 K isentropic surface is plotted such that only the tropospheric values between 0 and 1.5 PVU are color shaded. Higher values are not shaded so that white areas on the plots represent high PV stratospheric air. There are also small white areas of negative PV bordered by red color.

Let us take a closer look at Figure 3-6. For the moment we look separately at the eastern

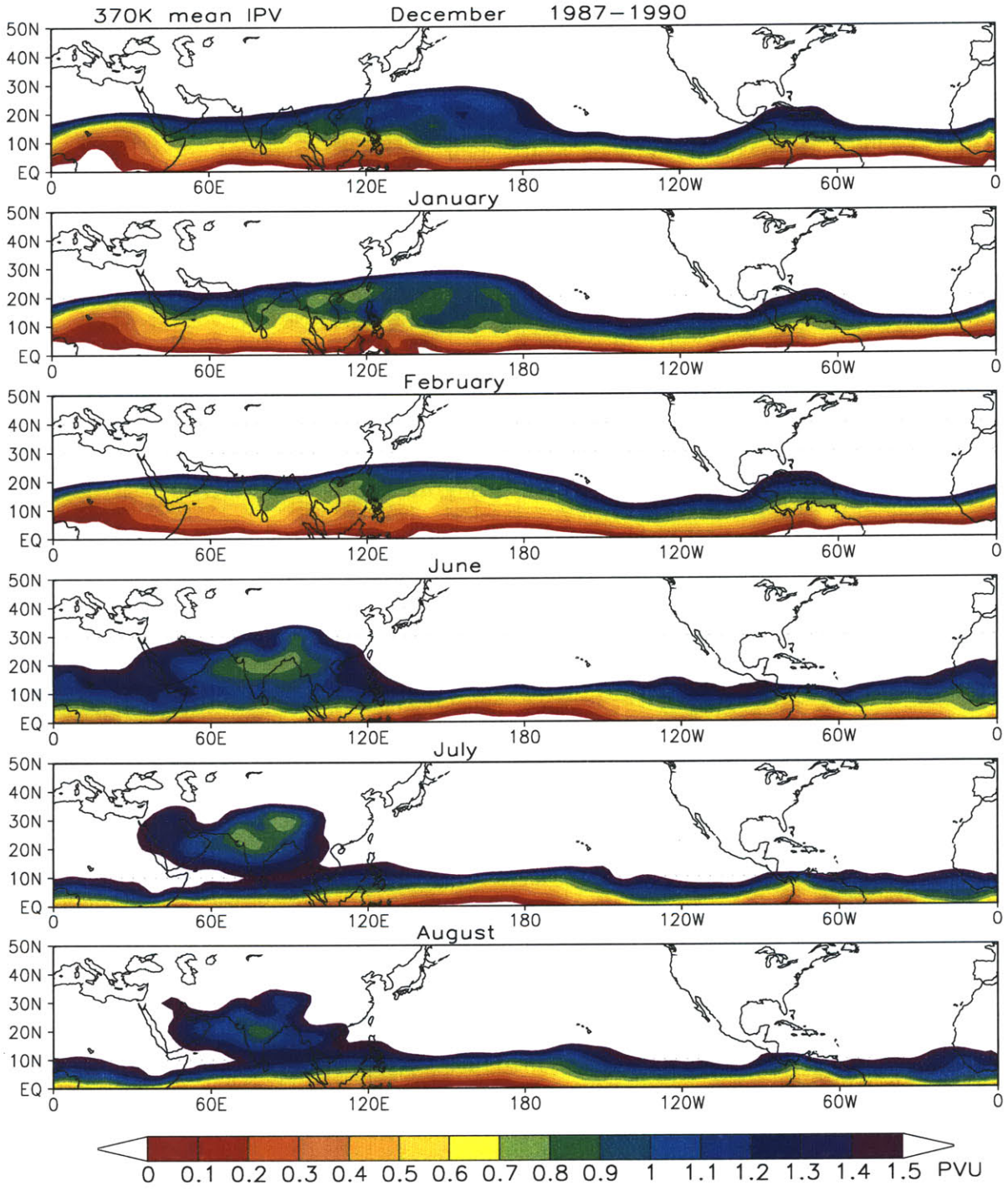

Figure 3-6: 1987-90 mean IPV field at 370 K for December to February (top three plots) and June to August (bottom three plots).

and western hemispheres. In the western hemisphere, low PV air is completely confined to the tropics, rarely crossing 10°N in summer months (three lower plots) and migrating bandwise more northwards (up to 20°N) in winter months (three upper plots). This also indicates that the tropical 370 K isentropic surface lies at lower altitudes in winter than in summer. The extension of low PV further north in winter than in summer is even more evident in the eastern hemisphere. However, one other feature, as we already noted in Figure 3-3, appears to be dominant in summer months, especially in July - the "blob" of low PV over south and southwest Asia. This low PV tropospheric air, associated with the anticyclonic divergent flow in the upper troposphere, is almost completely "isolated" in the surrounding high PV stratospheric air.

The next step is to analyze the time evolution of the IPV and streamfunction fields during summer. One practical way of looking at time evolution is to make time-longitude plots, also called Hovmöller diagrams. Hovmöller diagrams are a useful way to easily identify stationary features, propagation of features, oscillatory nature of the field, etc. Here, these diagrams are plotted such that time is on the ordinate, increasing from the top of the page downwards, and longitude, from 20°W to 180°E, is on the abscissa.

Figures 3-7 and 3-8 show the Hovmöller diagrams at 370 K for IPV and Montgomery streamfunction, respectively, averaged over the 10° latitudinal band between 25°N and 35°N. We consider every low PV feature in Figure 3-7 that separates from the main low PV body (which itself remains quasi-stationary) and propagates westward, as a possible candidate for eddy shedding. Two obvious features that fall into this category started around July 10 and July 17, 1990. The first of these two was a particularly clear example of eddy shedding. From now on, we shall refer to that event as the "sample case".

In Figures 3-9 to 3-14 we plot the time sequences of horizontal and vertical fields of the sample case eddy shedding event in July 1990. Figure 3-9 represents the time sequence plotted every 24 hours, from July 10 at 00 UTC to July 13 at 00 UTC, on the 370 K isentropic surface. The IPV field is color shaded as before. The contour lines are Montgomery streamfunction isolines with a minimum plotted (outer) isoline of 356000 $m^2\ s^{-2}$ and a contour interval of 250 $m^2\ s^{-2}$. In this event, what appears as one unified elongated anticyclonic vortex at the beginning of the shown time period, gradually becomes divided into two separate

vortices. We notice from Figure 3-9 that low IPV pulled away from the mother vortex (main low IPV body on the eastern side) and started to move southwestwards. After the filament reached 40°E at 00 UTC on July 11 (second plot), the secondary anticyclonic vortex was shed on the western side and propagated westwards, with its center reaching 30°E (southeast Mediterranean) by July 13 (fourth plot). After July 13, the secondary vortex existed for two more days. During that time it intensified and moved northward to the area of the strong westerly jet. Then, it was advected eastward by the jet and recaptured by the mother vortex. The divergent circulation in the upper troposphere is maintained by strong diabatic heating in the monsoonal circulation. The daughter vortex which was shed and moved westward, moved away from the source of its maintenance, as well. Its life is therefore not expected to be very long.

It is important to notice that in the days preceding the shedding, the anticyclone was stronger than usual. This can be seen from the Hovmöller diagram of M in Figure 3-8 and the horizontal sections of M and IPV (not shown). In addition, the anticyclone was becoming more and more elongated (the eccentricity of the isolines of M in the central region especially increased). The flow became almost parallel, i.e. almost purely westerly in the northern part and almost purely easterly in the southern part of anticyclone. The almost zonal flow suggests one possible explanation for why the eddy shedding occurred. In these circumstances we may apply the criteria for instability in the parallel (shear) flow locally - the change of sign in the potential vorticity gradient implies that the necessary condition for instability has been met. As a consequence, eddy shedding occurs, and by July 13 we notice two separate anticyclones in Figures 3-9 to 3-11. The existence of this dynamically unstable condition, which is necessary to generate the transient eddies in the observations, agrees well with the results that Hsu (1998) obtained in her numerical model.

The eddy shedding phenomenon is relatively shallow. Figures 3-13 and 3-14 show the vertical structure of the deviation from the zonal mean of the IPV and M fields in our sample case. In these figures, vertical cross sections are latitudinally averaged between 27.5°N and 37.5°N. The negative values of the deviation from the zonal mean, in Figure 3-13 arise because the potential vorticity field has much lower values in the region of interest compared to other longitudes. To stress the important areas, the values smaller than -0.5 PVU are

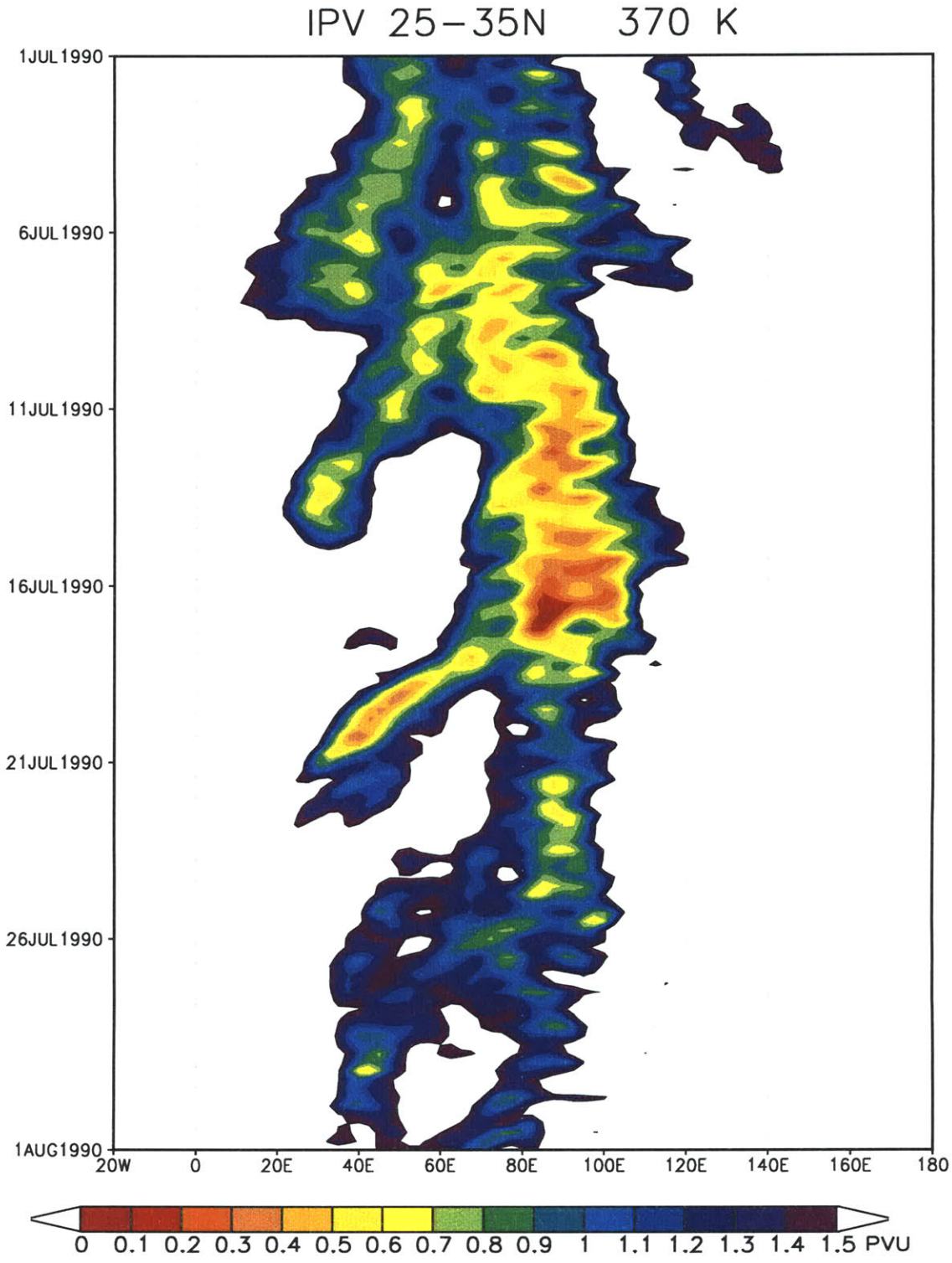

Figure 3-7: Hovmöller diagram of IPV for July 1990 at 370 K, averaged over the 10° latitudinal band between 25°N and 35°N.

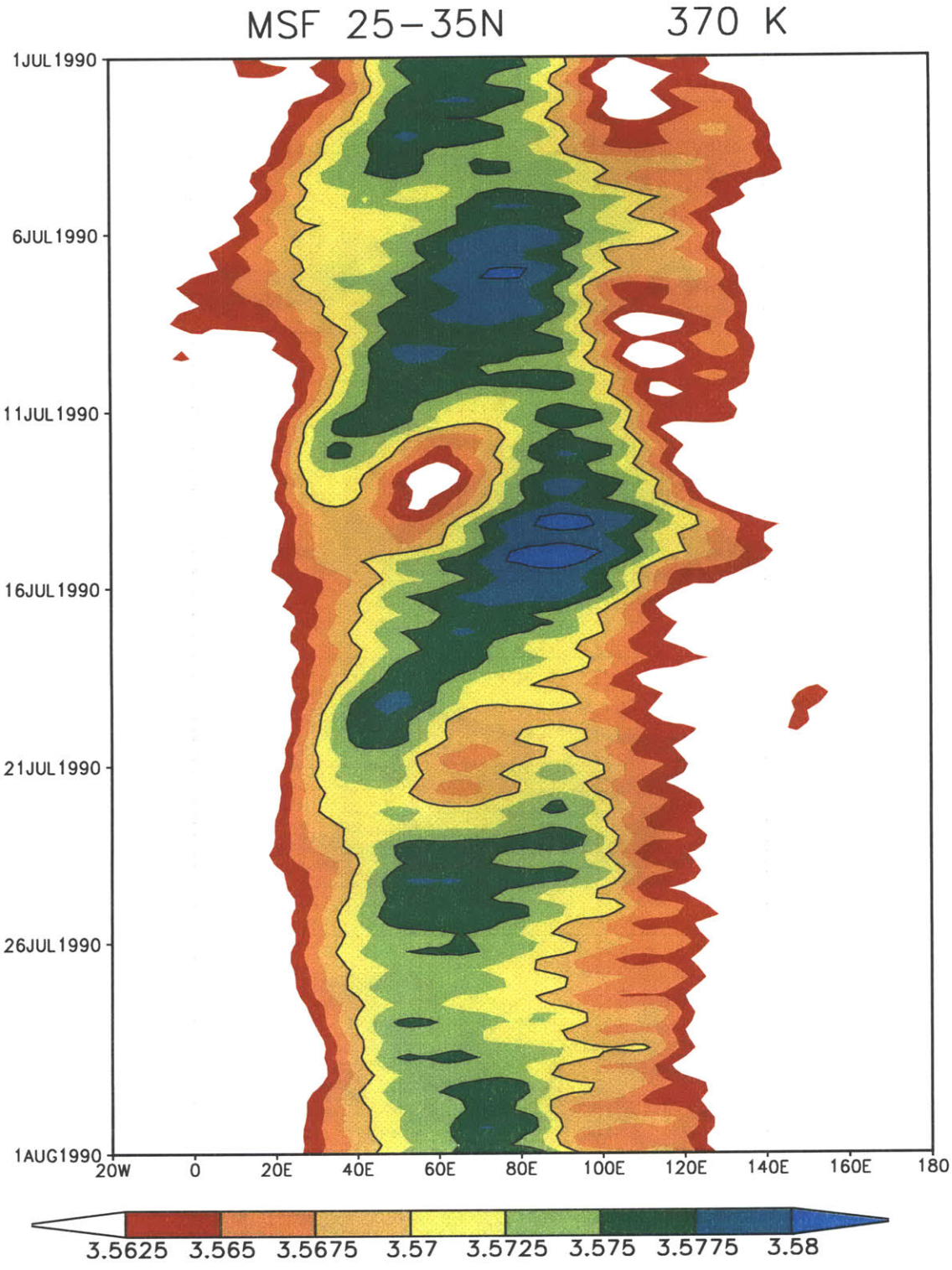

Figure 3-8: Hovmöller diagram of Montgomery streamfunction for July 1990 at 370 K averaged over the 10° latitudinal band between 25°N and 35°N.

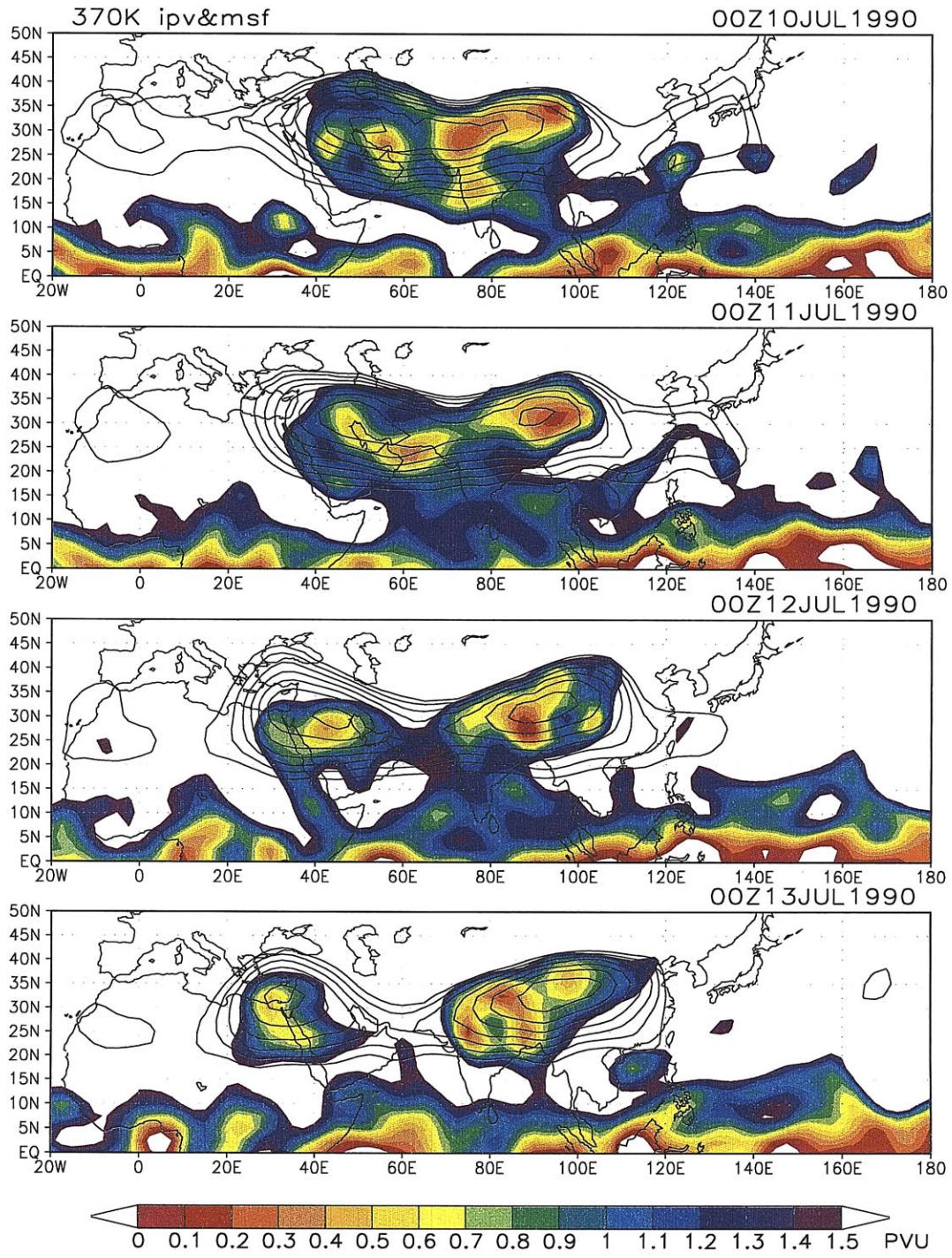

Figure 3-9: Time sequence of IPV (color shading) and M (line contours) fields at 370 K given in successive 24-hour intervals from 00 UTC July 10 to 00 UTC July 13, 1990. Minimum value of displayed contour lines is 356000 m^2 s^{-2}. Contour line interval is 250 m^2 s^{-2}.

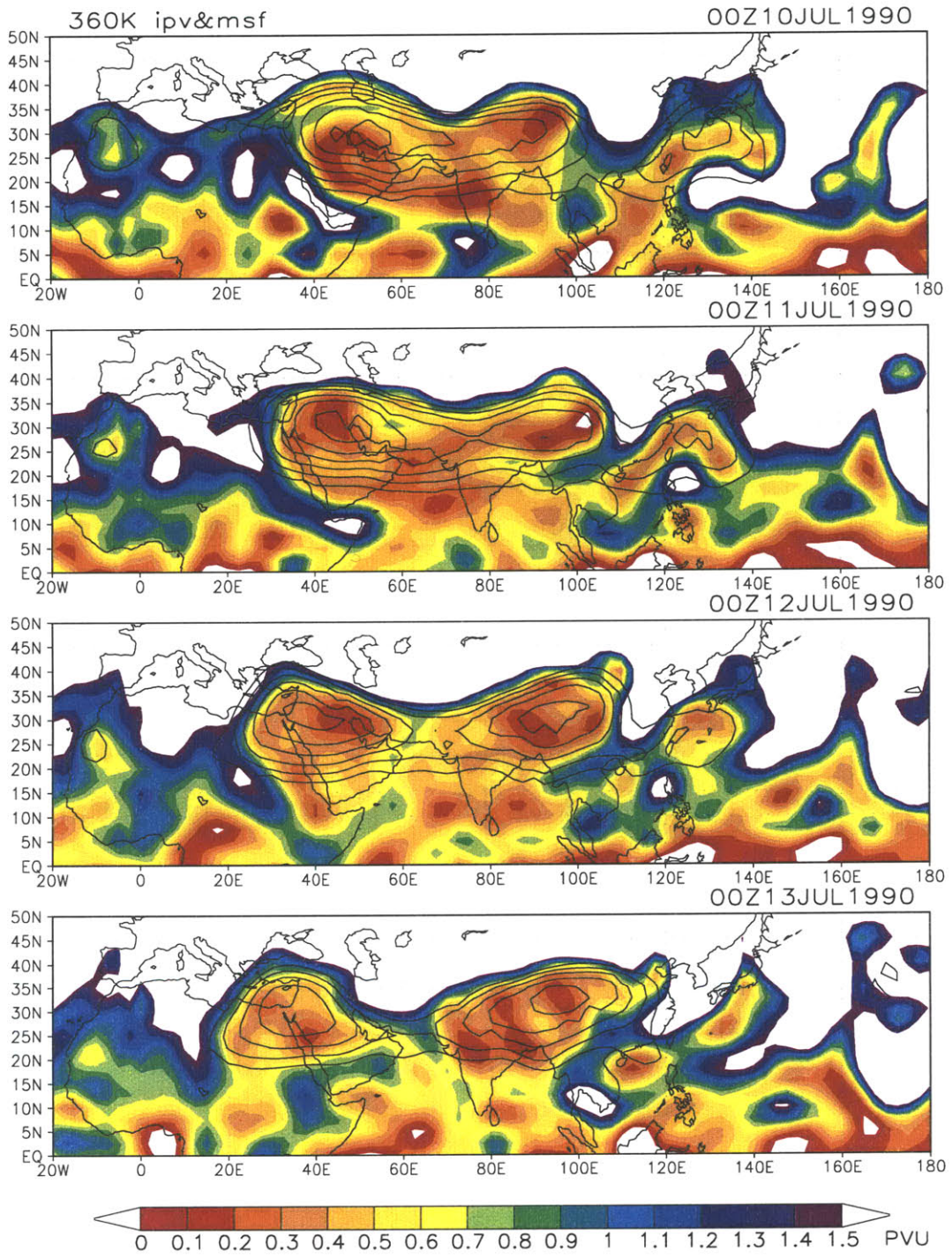

Figure 3-10: Time sequence of IPV (color shading) and M (line contours) fields at 360K given in successive 24-hour intervals from 00 UTC July 10 to 00 UTC July 13, 1990. Minimum value of displayed contour lines is 350500 $m^2\ s^{-2}$. Contour line interval is 250 $m^2\ s^{-2}$.

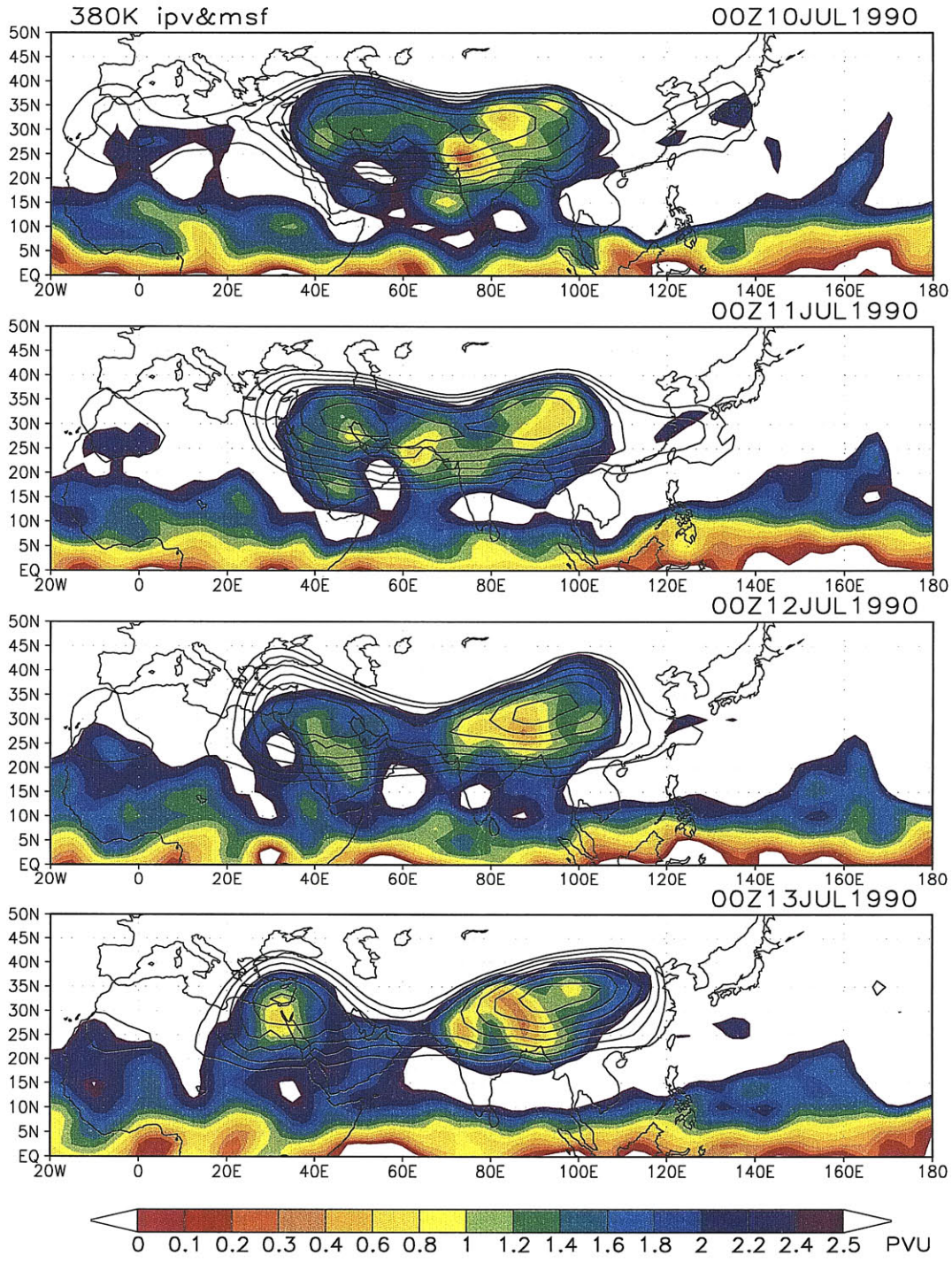

Figure 3-11: Time sequence of IPV (color shading) and M (line contours) fields at 380K given in successive 24-hour intervals from 00 UTC July 10 to 00 UTC July 13, 1990. Minimum value of displayed contour lines is 361500 m^2 s^{-2}. Contour line interval is 250 m^2 s^{-2}.

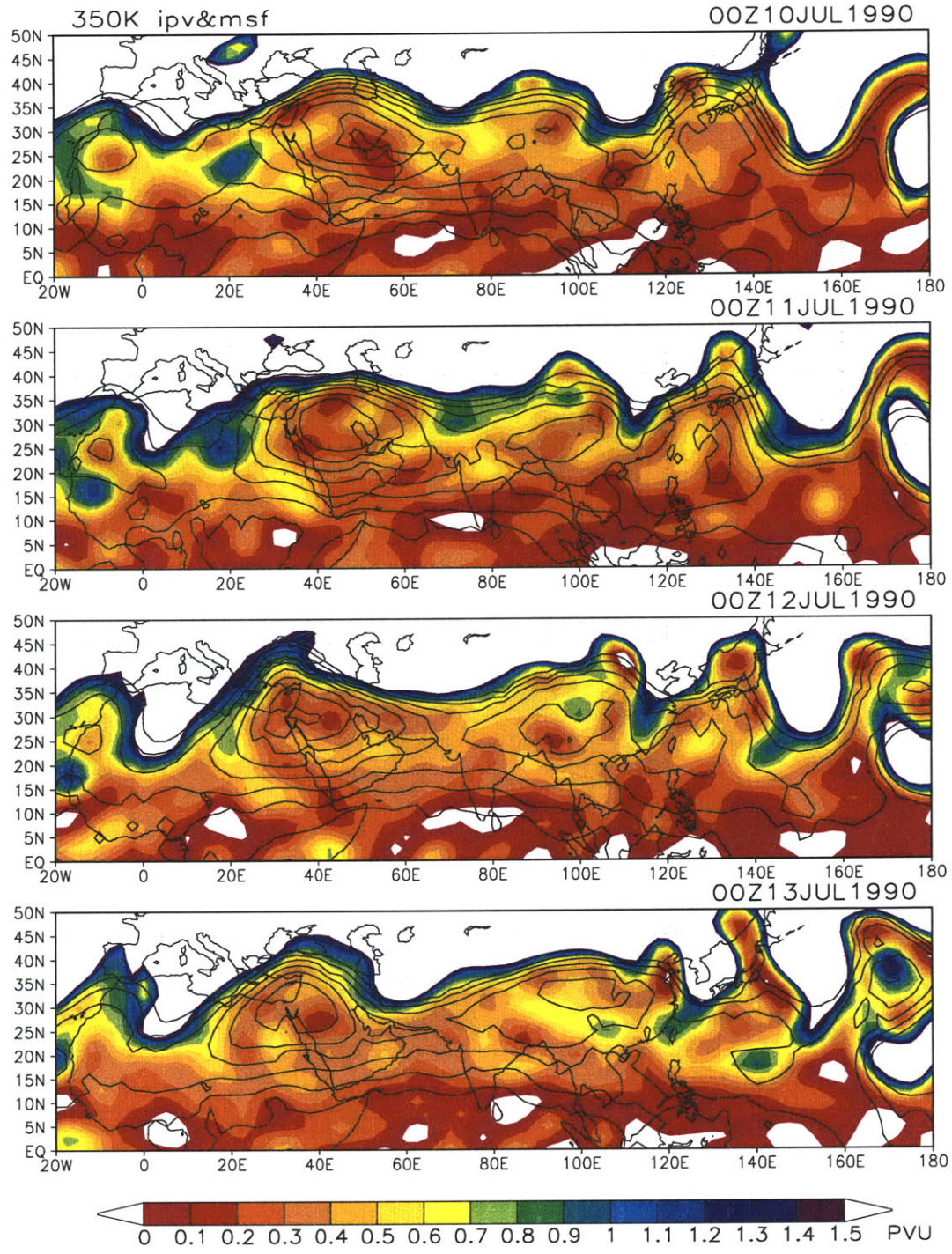

Figure 3-12: Time sequence of IPV (color shading) and M (line contours) fields at 350K given in successive 24-hour intervals from 00 UTC July 10 to 00 UTC July 13, 1990. Minimum value of displayed contour lines is 343500 m^2 s^{-2}. Contour line interval is 250 m^2 s^{-2}.

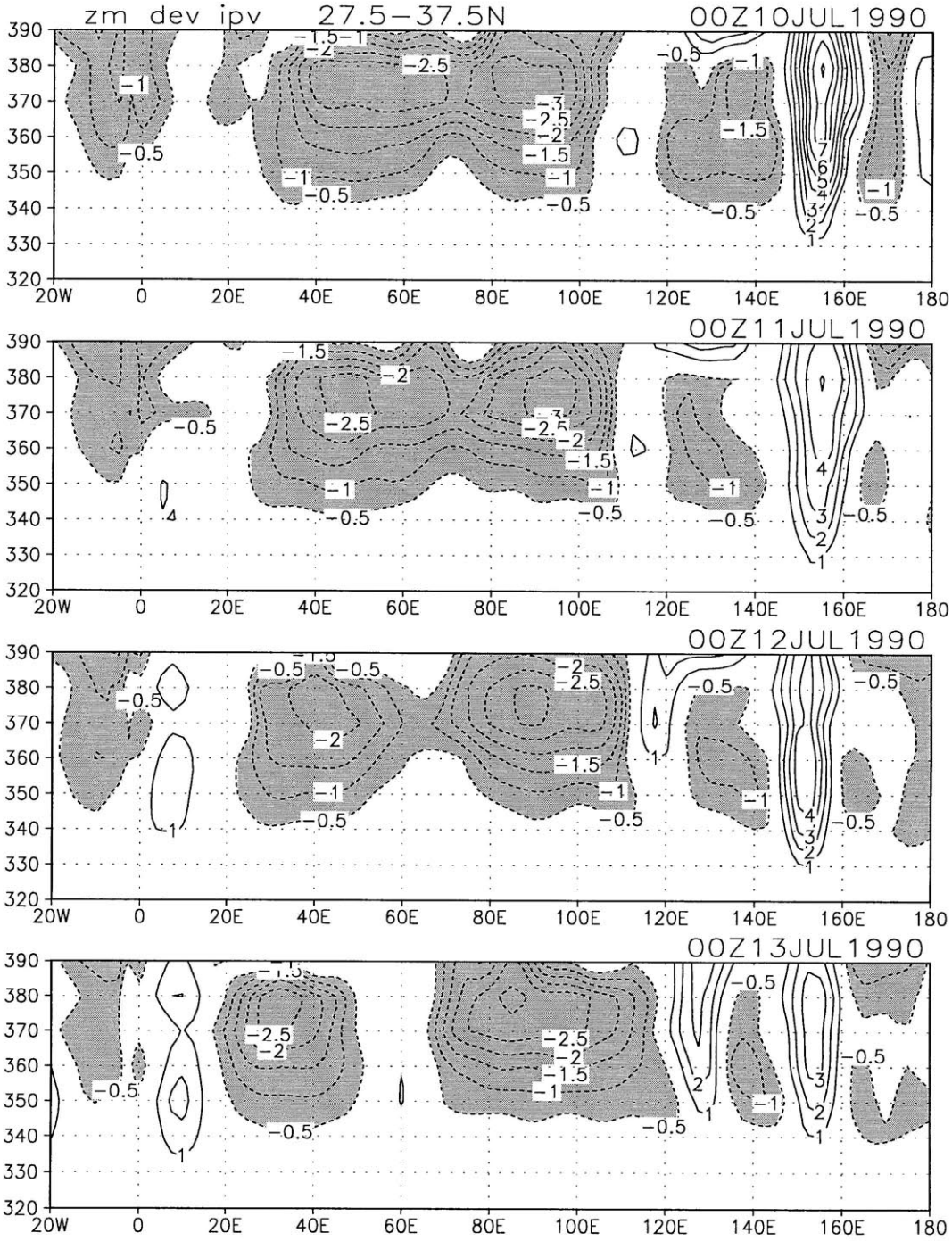

Figure 3-13: Time sequence of vertical cross sections of the perturbation from the zonal mean of IPV, latitudinally averaged between 27.5°N and 37.5°N, given in successive 24-hour intervals from 00 UTC July 10 to 00 UTC July 13, 1990. The values smaller than -0.5 PVU are shaded.

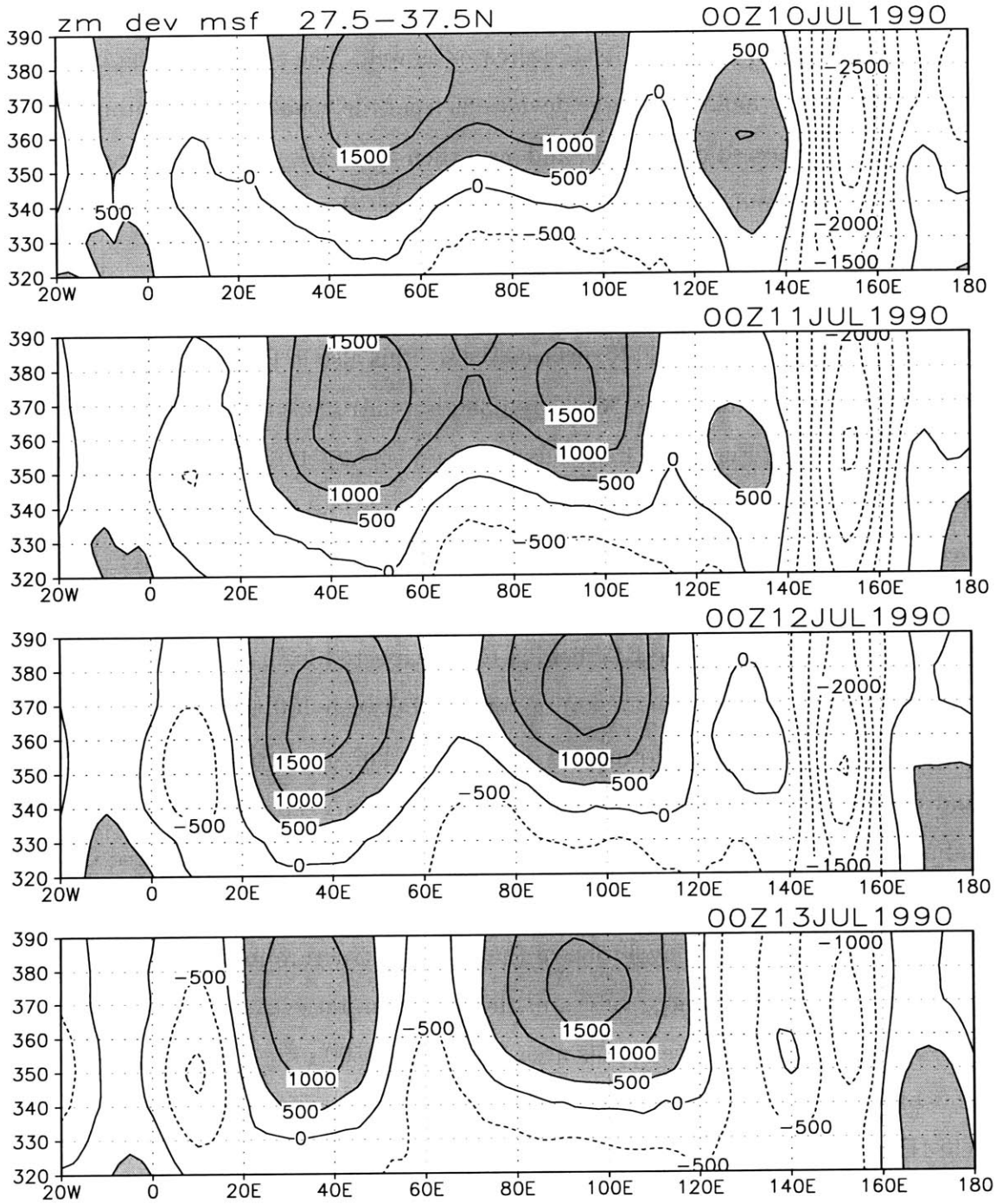

Figure 3-14: Time sequence of vertical cross sections of the perturbation from the zonal mean of M, latitudinally averaged between 27.5°N and 37.5°N, given in successive 24-hour intervals from 00 UTC July 10 to 00 UTC July 13, 1990. The values greater than 500 m^2s^{-2} are shaded.

shaded. The strongest deviation from the zonal mean is found close to the 370 K level. The magnitude of the deviation from the zonal mean decreases downward but at the same time the absolute value of the PV field itself decreases as well. The eddy shedding in Figure 3-13 is easily recognized by looking at large deviations from the zonal mean. Contour lines of -1.5 and -2 PVU are connected on July 10, and even then -2.5 PVU contour is almost connected. With time, the -1.5 and -2 PVU contours separate as the western part sheds and moves westward, causing the -1.5 and -2 PVU contours to separate.

From Figure 3-13, eddy shedding in the IPV field is confined to the layer between the tropopause (~380 K) and the 360 K surface. We see this also in Figures 3-10 and 3-11, which show the IPV and M fields at the 360 K and 380 K isentropic surfaces. Note that the range of shaded PV values in Figure 3-11 extends to 2.5 PVU. At 350 K (Figure 3-12), the low IPV of the monsoonal anticyclone is not separated from the low IPV in the tropics. However, the shedding in the M field is seen even at these lower levels (down to 350 K). Although the shedding is still shallow in the streamfunction field, the fact that it appears deeper in the streamfunction field than in the IPV field is to be expected from the invertibility principle. The expected depth (H) is about 7 km or roughly between 100 and 300 mb. ($H = \frac{L}{L_R} H_R$, where the Rossby radius of deformation $L_R \approx 3000$ km, the tropopause height $H_R \approx 15$ km, and the horizontal extent of the eddies $L \approx 1500$ km.) Therefore, the shedding in the streamfunction field is observed in Figure 3-12 (350 K), but it is not observed on the levels below that.

In Figure 3-14, we see the evolution of the vertical structure in the M field. The Montgomery streamfunction has large values in the monsoon anticyclone, so that the deviation from the zonal mean is positive in this area, exceeding 1500 $m^2\ s^{-2}$ near the 370 K surface. Figure 3-14 also shows that the shedding in the streamfunction field is deeper than in the PV field (Figure 3-13).

Eddy shedding in the sample case occurred when the primary vortex achieved a regular elongated elliptical shape with an almost parallel flow. Therefore, the sample case almost perfectly corresponds to the modeled flow in Hsu (1998). However, the atmosphere rarely strictly conforms to any simple theoretical model and there are always variations and slight differences. All other cases that we examine next have many similarities with the modeled

flow and our sample case from atmospheric data, but some differences as well.

Figures 3-15 to 3-18 represent small versions of Hovmöller diagrams of IPV and M at 370 K for the 10° latitudinal band between 25°N and 35°N for June (top panels), July (middle panels) and August (bottom panels) of four analyzed years. Years 1987 and 1988 are shown in Figures 3-15 and 3-17, while years 1989 and 1990 are shown in Figures 3-16 and 3-18. These plots show just the overall pattern of IPV and M fields throughout the summer on the selected isentropic level of 370 K. Detailed structures will be shown in the next section on the time sequences of selected events.

From Figures 3-15 and 3-16 we may immediately notice the following: from June to August, at the isentropic level of 370 K, the bulk of the low PV (tropospheric) air in the 25°-35°N latitudinal band is confined between the longitudes of 20°E and 120°E. There are periods of time when the low PV strip remained stationary, indicating the presence of the anticyclonic vortex at almost the same position for several days. However, we also see a number of westward-propagating features and a few eastward-propagating features. We notice that most of the westward moving features coexisted with the almost stationary low PV body, and these were actually the eddy shedding events. The eddies that are shed are most often smaller than the eddies from which they are detached. Although smaller, they are still large with diameters of 2000 to 3000 km. There were also two westward moving features which did not have a low PV body counterpart on the east (August 1987 and July 1989). The anticyclone did not break up in these two cases but it propagated westward as a whole.

3.3 Other cases of eddy shedding

The sample case of eddy shedding in the upper tropospheric monsoonal circulation that we presented was the clearest example of this phenomenon in the four years we analyzed. In this section we present all other eddy shedding cases that happened in July 1987 to 1990, as well as other characteristics in the evolution of the chosen meteorological fields. All these are depicted using the time sequences of IPV and M fields at 370 K (we showed four different levels for the sample case) and time sequences of vertical cross sections of 10° latitudinally

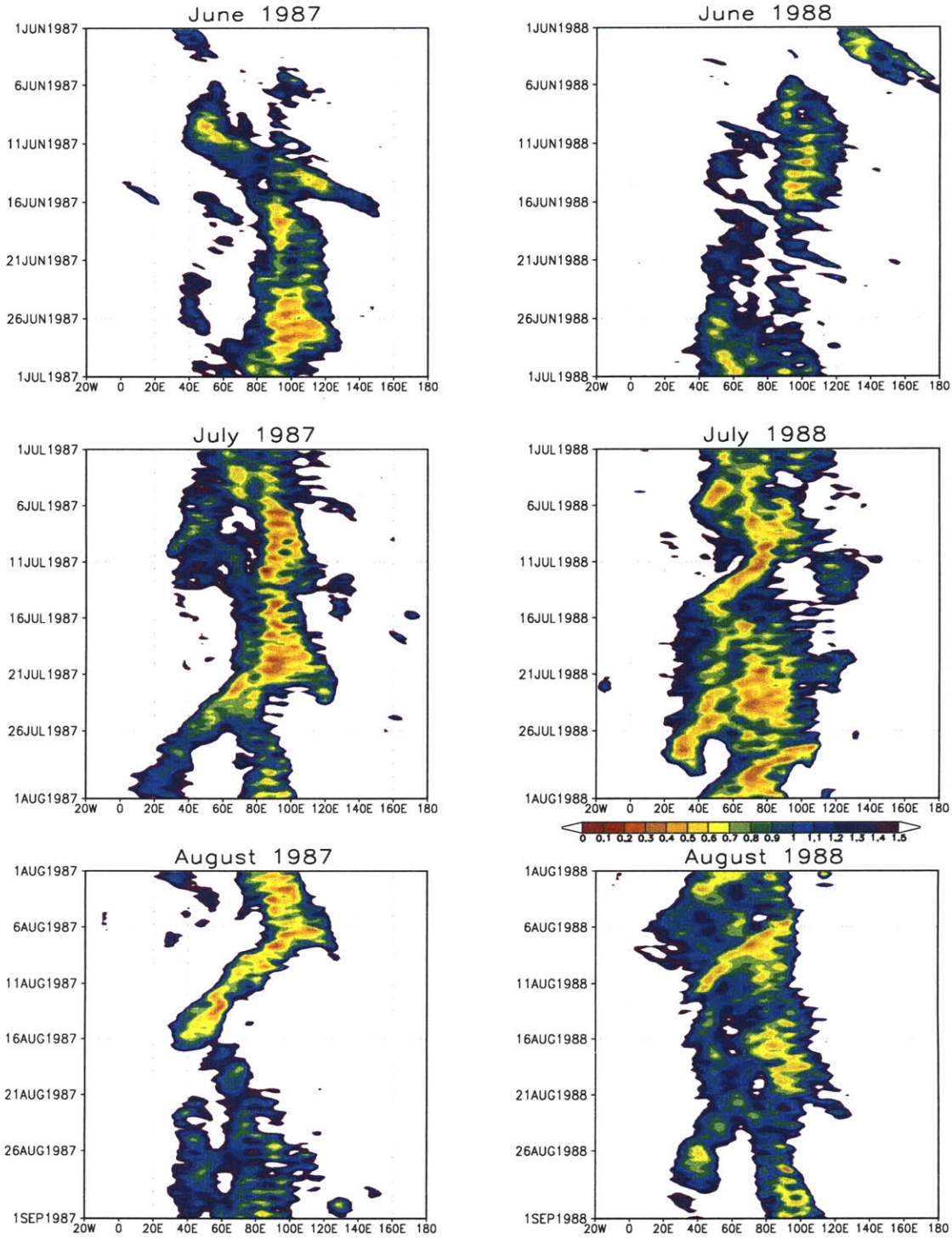

Figure 3-15: Hovmöller diagrams of IPV at 370 K averaged over the 10° latitudinal band between 25°N and 35°N, for June (top), July (middle), and August (bottom) of 1987 (left) and 1988 (right).

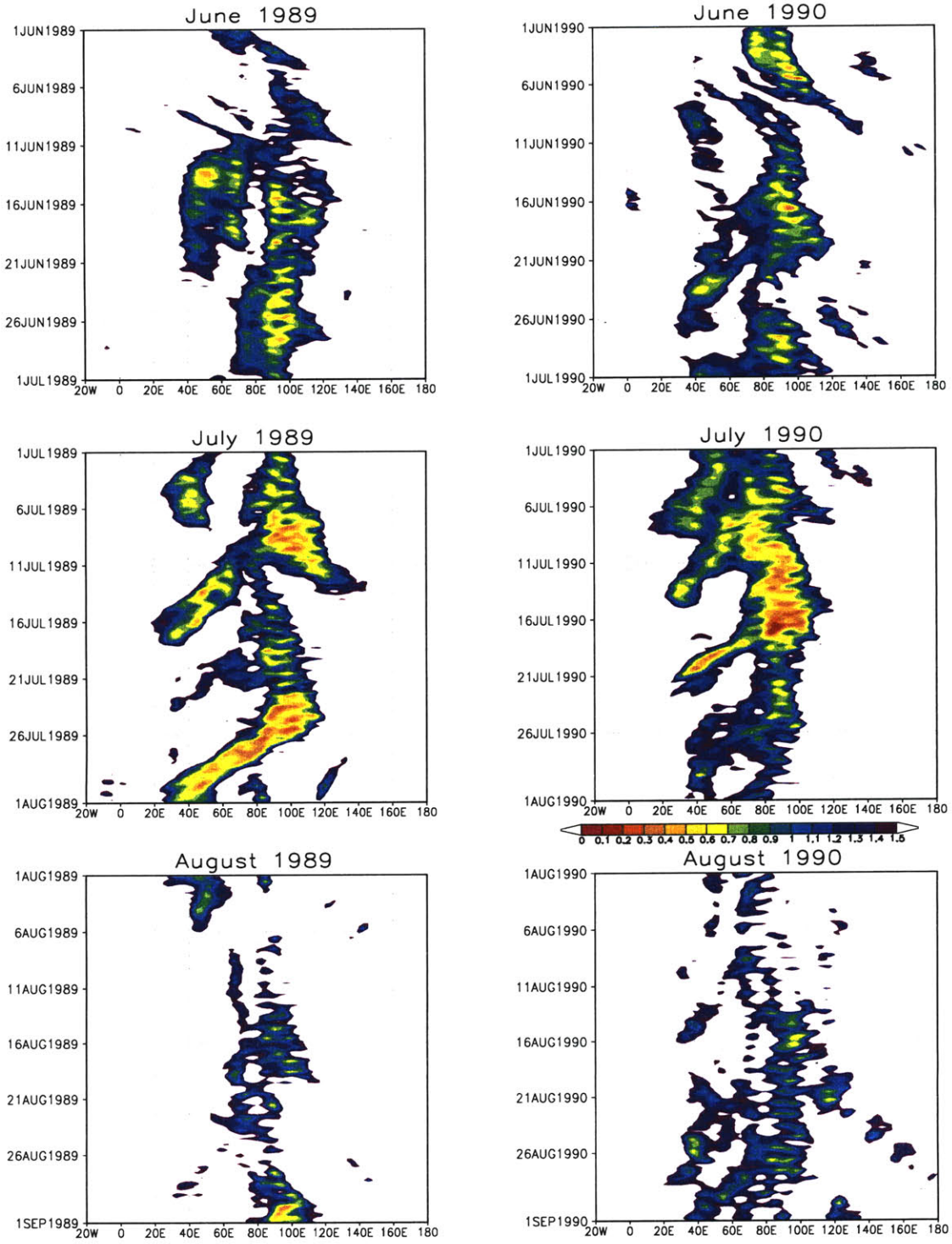

Figure 3-16: Hovmöller diagrams of IPV at 370 K averaged over the 10° latitudinal band between 25°N and 35°N, for June (top), July (middle), and August (bottom) of 1989 (left) and 1990 (right).

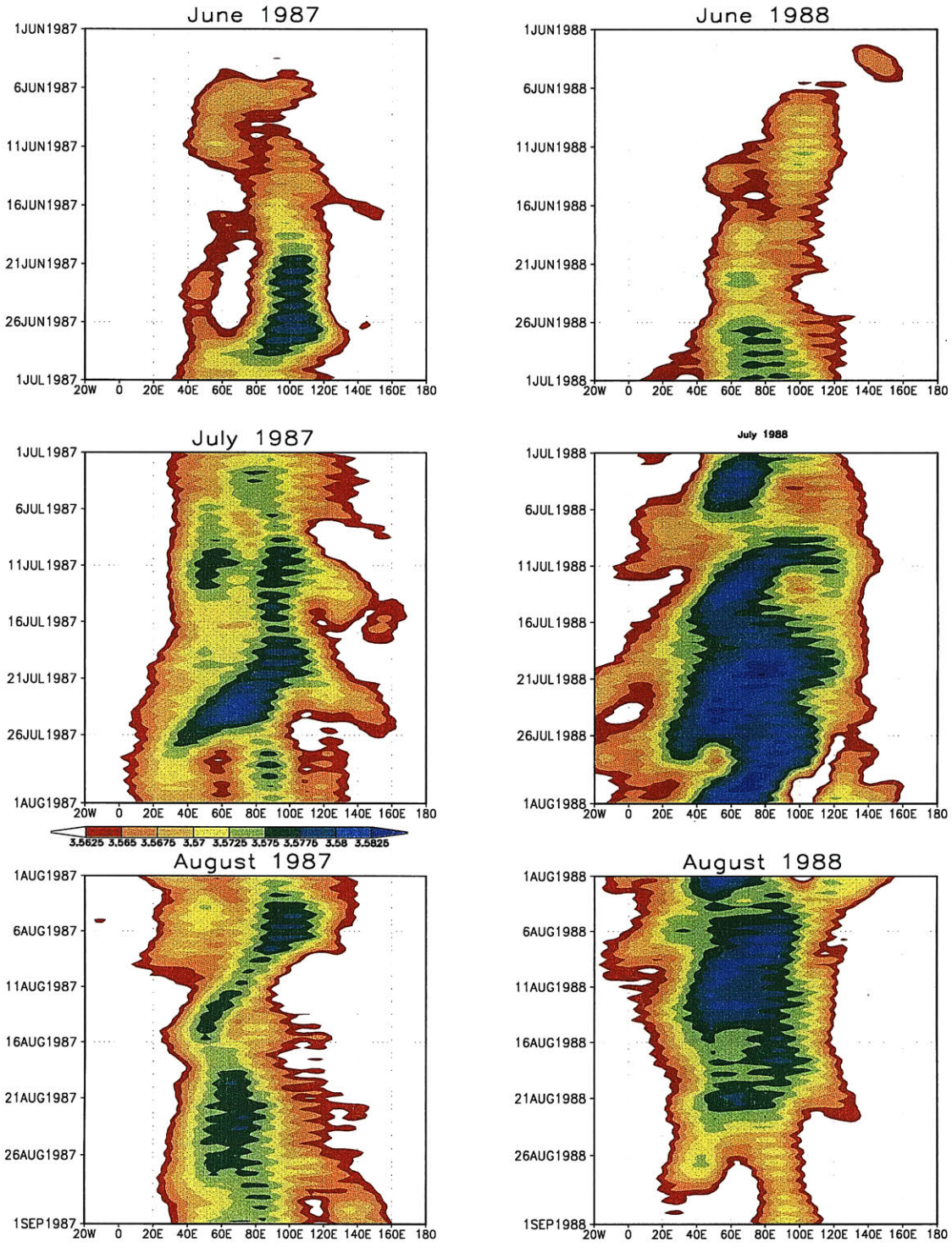

Figure 3-17: Hovmöller diagrams of M at 370 K averaged over the 10° latitudinal band between 25°N and 35°N, for June (top), July (middle), and August (bottom) of 1987 (left) and 1988 (right).

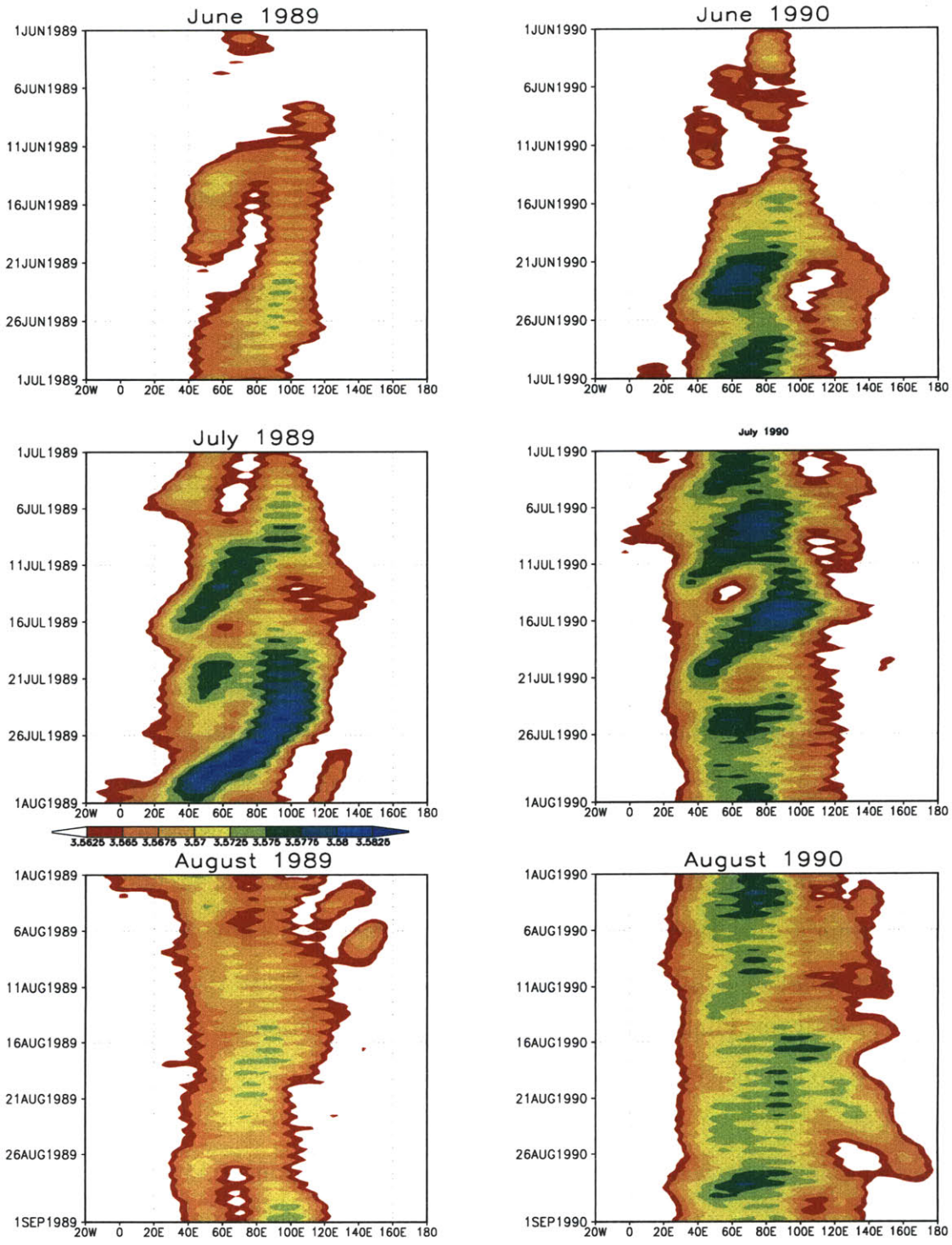

Figure 3-18: Hovmöller diagrams of M at 370 K averaged over the 10° latitudinal band between 25°N and 35°N, for June (top), July (middle), and August (bottom) of 1989 (left) and 1990 (right).

averaged zonal deviations of IPV or M.

3.3.1 July 1987

July 1987 was marked by two eddy shedding events. The first one is shown in Figures 3-19 and 3-20, and it was not a very clear example. The second one is shown in Figures 3-21 and 3-22.

The upper tropospheric anticyclone at the beginning of July 1987 was rather elongated and moderately strong. It was centered about 80°E and 25°N. For the first few days of the month, the winds were almost pure westerlies in the northern part of the anticyclone and pure easterlies in the southern part. The change of sign in the gradient of potential vorticity in this parallel flow regime indicates the existence of the necessary condition for dynamical instability. From what we have seen so far in the sample case, we may expect to see eddy shedding occurring at some later time of the month. Actually, what started on July 5 (first plot in Figure 3-19) may be considered as an eddy shedding event since we observed two cells in the center of the large scale anticyclonic circulation. Figures 3-19 and 3-20 shows the first part of the ten day period when the two cells in the streamfunction field existed. These figures show time sequences of the horizontal and vertical cross sections, in time steps of 36 hours. However, this case also differed in several aspects from what we have described so far as an eddy shedding event. Namely, the two cells remained at almost the same position during their lifetime, i.e. the western cell did not move westward with time. Another important difference was related to the IPV field. At first, it looked like the other clear eddy shedding events. From the horizontal section we see how the low IPV (yellow area) strip stretched to the west (second plot) and the new low PV cell formed on the western side (third plot). However, later on the western low PV cell was broken and did not last as long as the M western cell. From the vertical section of M we also notice the transition from a one-vortex to a two-vortex structure. The strength and the depth of both cells varied with time.

The anticyclone regained its unified form by the middle of the month, becoming rounder (the isolines of the streamfunction achieving elliptical shapes of lower eccentricity). After that short period the isolines became more elongated once more and the vortex became

stronger, with its center moving westward. As a result, on July 26 another eddy shedding event started. From the time sequence with a 24 hours interval shown in Figures 3-21 and 3-22, we see that the elongated anticyclonic cell centered around 60°E and 30°N on July 25 (upper plot) started to gradually break into two entities (July 26 - second plot). On July 27 and 28, the mother vortex remained on the eastern side, building up with time while the daughter vortex moved westward and weakened. This eddy shedding event ended three days after the last time plot shown (bottom plot). This was one more case in which the low IPV of the weakened daughter vortex was advected by the westerly jet toward the mother vortex.

3.3.2 July 1988

In summer 1988, the upper tropospheric circulation was much stronger than in the other three analyzed years. For the first five days of July, the flow had a strong anticyclonic circulation centered at 60°E and 30°N and also had rather low eccentricity. After July 5, the anticyclone became weaker and much more elongated. The center itself gradually moved eastwards to around 80°E and the whole system acquired much larger dimensions than usual. From the plot on the top of Figure 3-23 we see that the streamlines were almost zonal, and so was the wind direction in most of the area. However, this was not a typical case of eddy shedding. In this case, the main anticyclonic cell remained almost at the same position, losing much of its eccentricity by July 12 (bottom plot) and residing in the area of the climatological mean position of the anticyclone. At the same time, on the northeastern end of the large scale anticyclonic circulation, we observe a strong easterly jet and a filament of low PV (upper plot) which rolled up in the anticyclonic direction. By July 11 (third plot), it built up into the secondary anticyclonic vortex which lasted for three days and then vanished.

After this unusual event, by mid-July the anticyclone regained its (unusual) strength and large eccentricity and remained like that for the following 10 days. It was particularly strong around July 20. This rather long period of such a strong and large scale anticyclonic circulation gradually started to change around July 25, resulting in another eddy shedding event. At that time, the center of the large scale anticyclone shifted slightly northeastward and a daughter vortex shed on the western side. An eighteen-hour time sequence of this

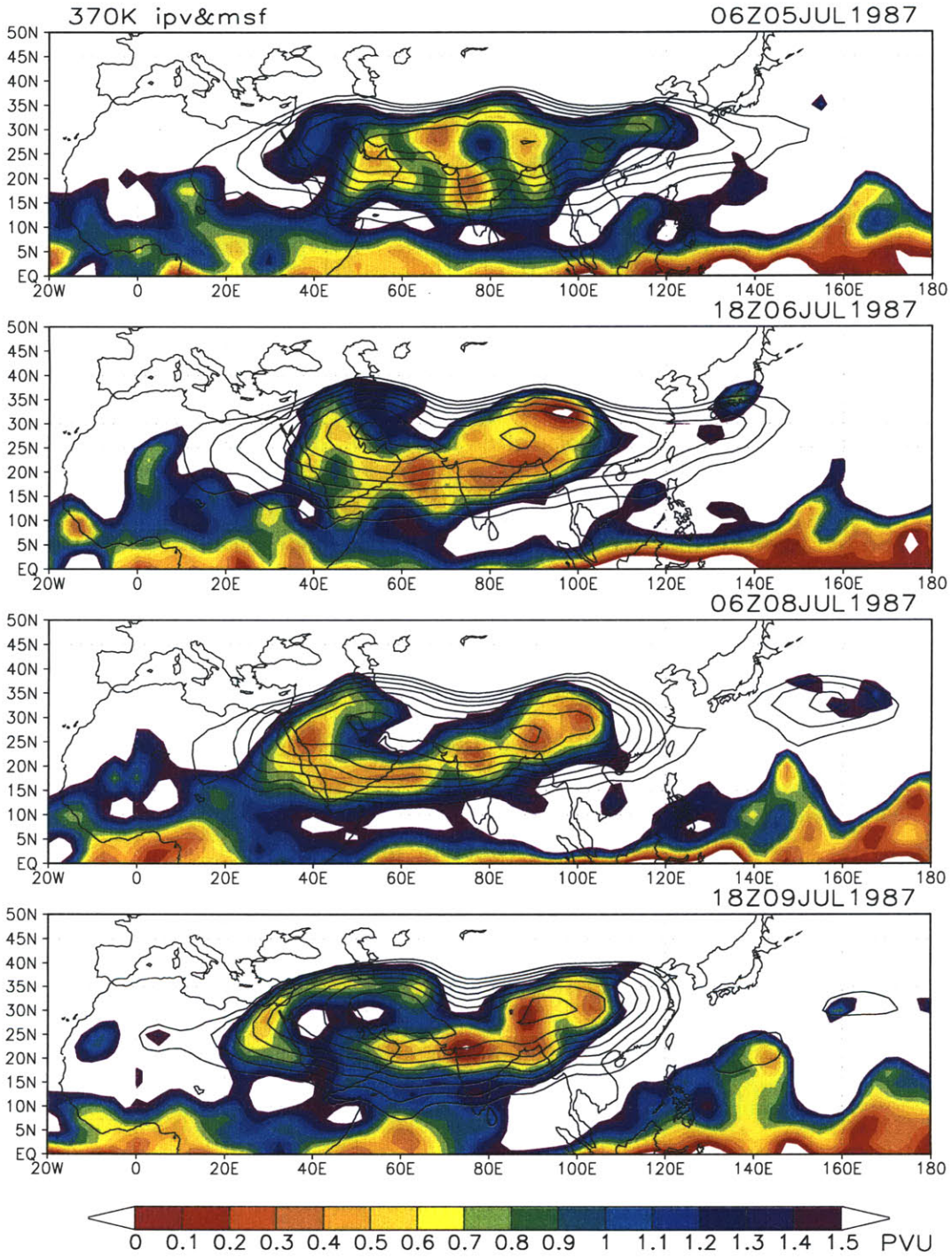

Figure 3-19: Time sequence of IPV (color shading) and M (line contours) fields at 370 K given in successive 36-hour intervals from 06 UTC July 5 to 18 UTC July 9, 1987. Minimum value of displayed contour lines is 356000 m^2 s^{-2}. Contour line interval is 250 m^2 s^{-2}.

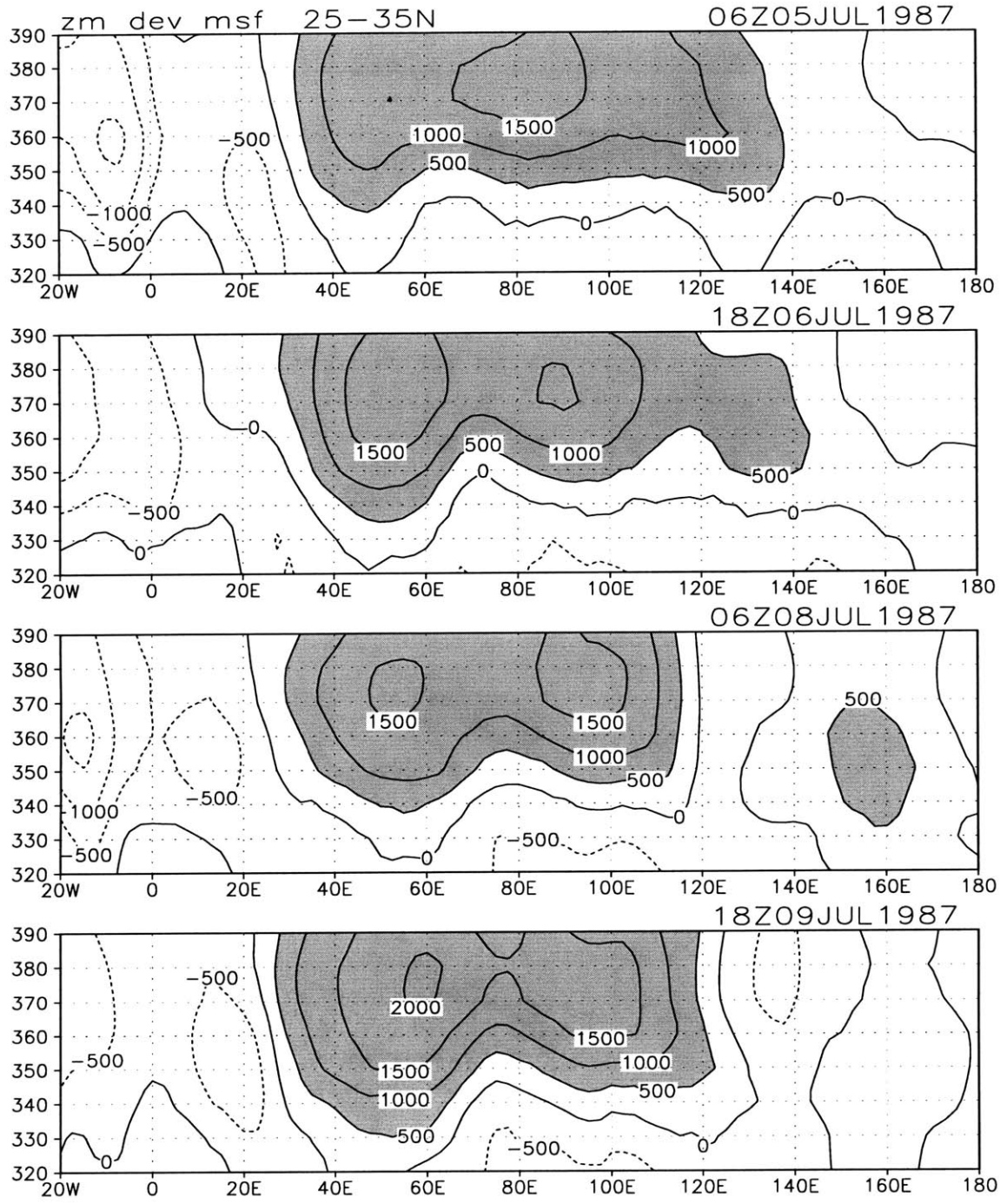

Figure 3-20: Time sequence of vertical cross sections of the perturbation from the zonal mean of M, latitudinally averaged between 25°N and 35°N, given in successive 36-hour intervals from 06 UTC July 5 to 18 UTC July 9, 1987. The values greater than 500 m^2s^{-2} are shaded.

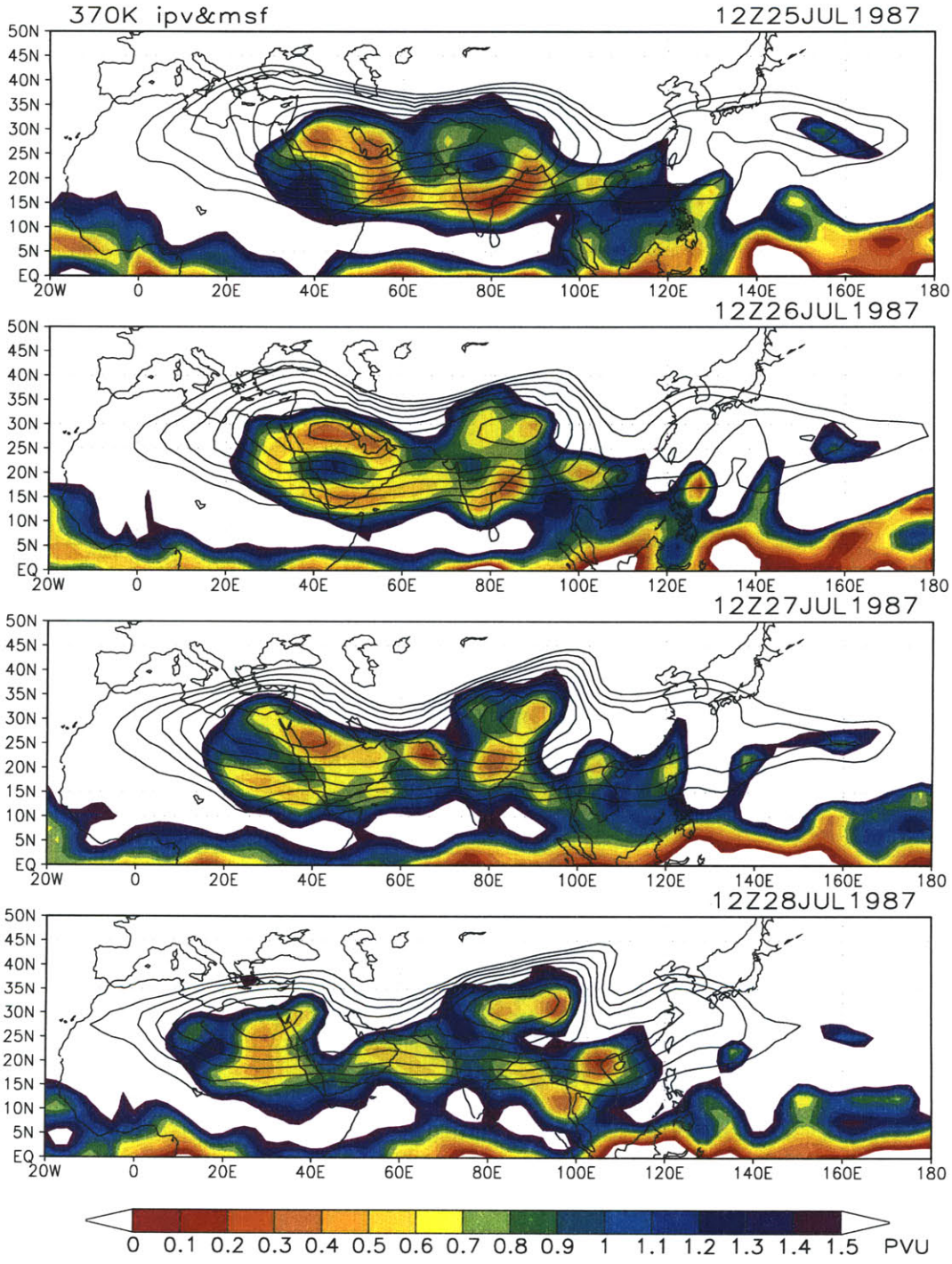

Figure 3-21: Time sequence of IPV (color shading) and M (line contours) fields at 370K given in successive 24-hour intervals from 12 UTC July 25 to 12 UTC July 28, 1987. Minimum value of displayed contour lines is 356000 m^2 s^{-2}. Contour line interval is 250 m^2 s^{-2}.

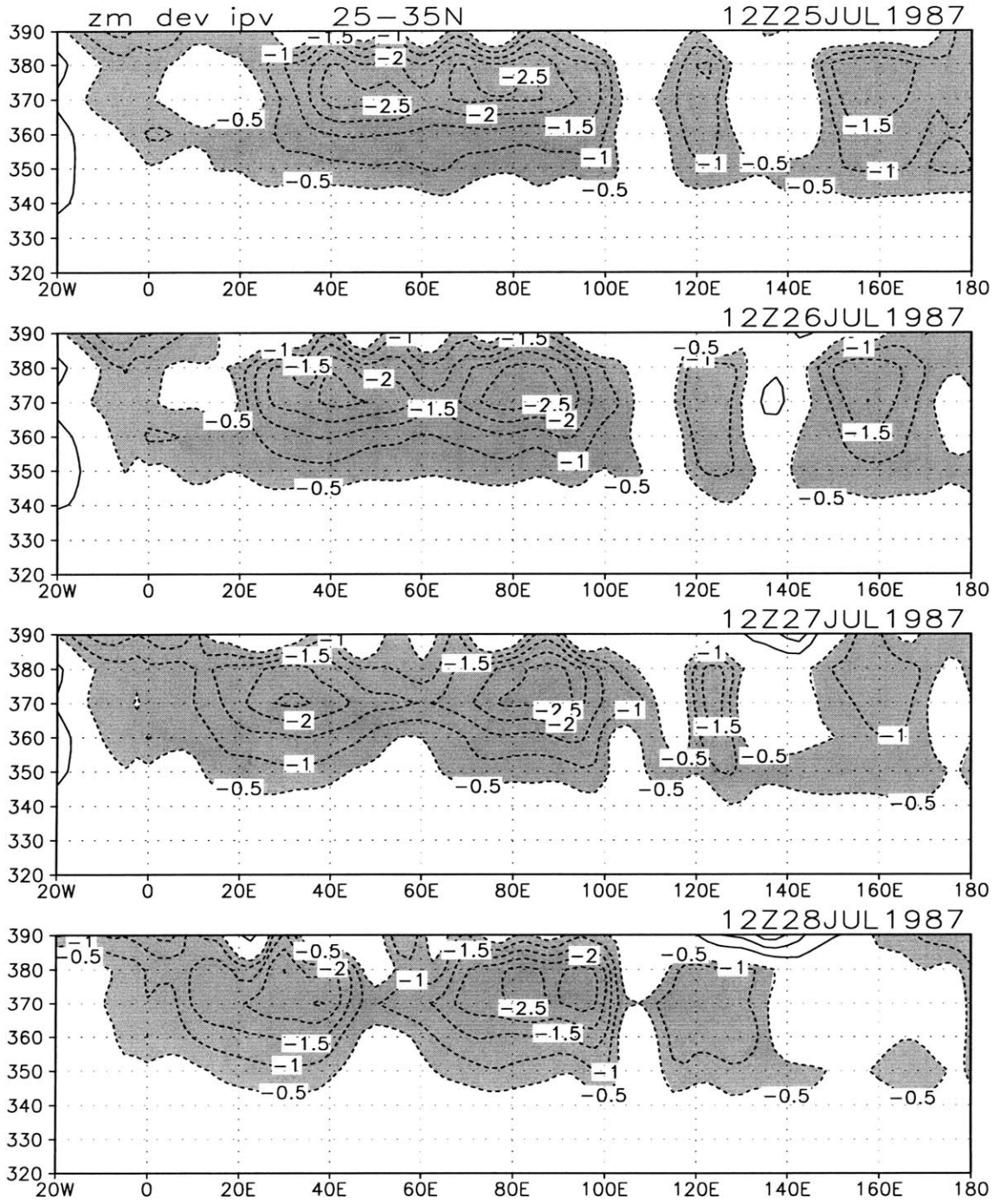

Figure 3-22: Time sequence of vertical cross sections of the perturbation from the zonal mean of IPV, latitudinally averaged between 25°N and 35°N, given in successive 24-hour intervals from 12 UTC July 25 to 12 UTC July 28, 1987. The values smaller than -0.5 PVU are shaded.

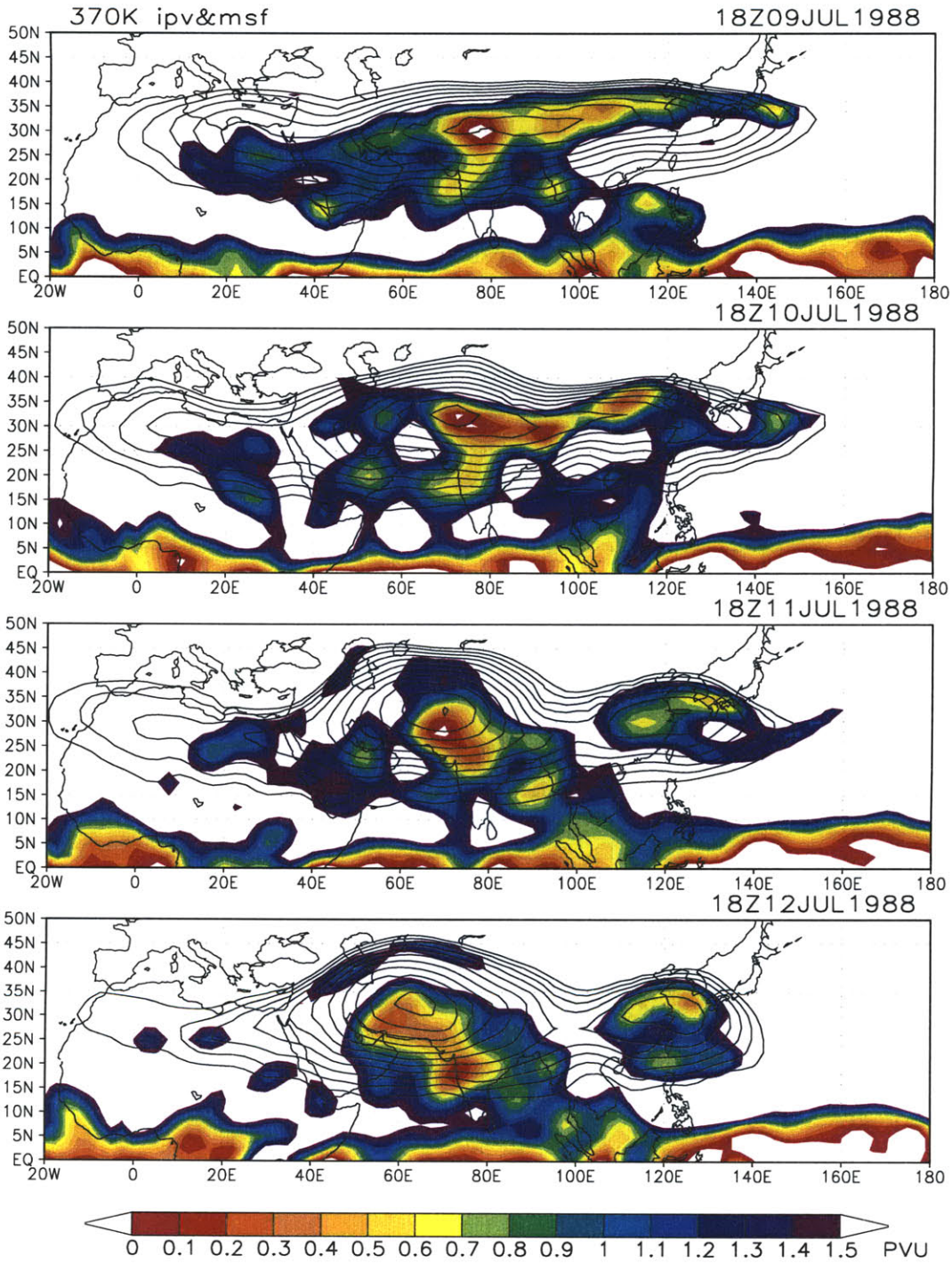

Figure 3-23: Time sequence of IPV (color shading) and M (line contours) fields at 370 K given in successive 24-hour intervals from 18 UTC July 9 to 18 UTC July 12, 1988. Minimum value of displayed contour lines is 356000 $m^2\ s^{-2}$. Contour line interval is 250 $m^2\ s^{-2}$.

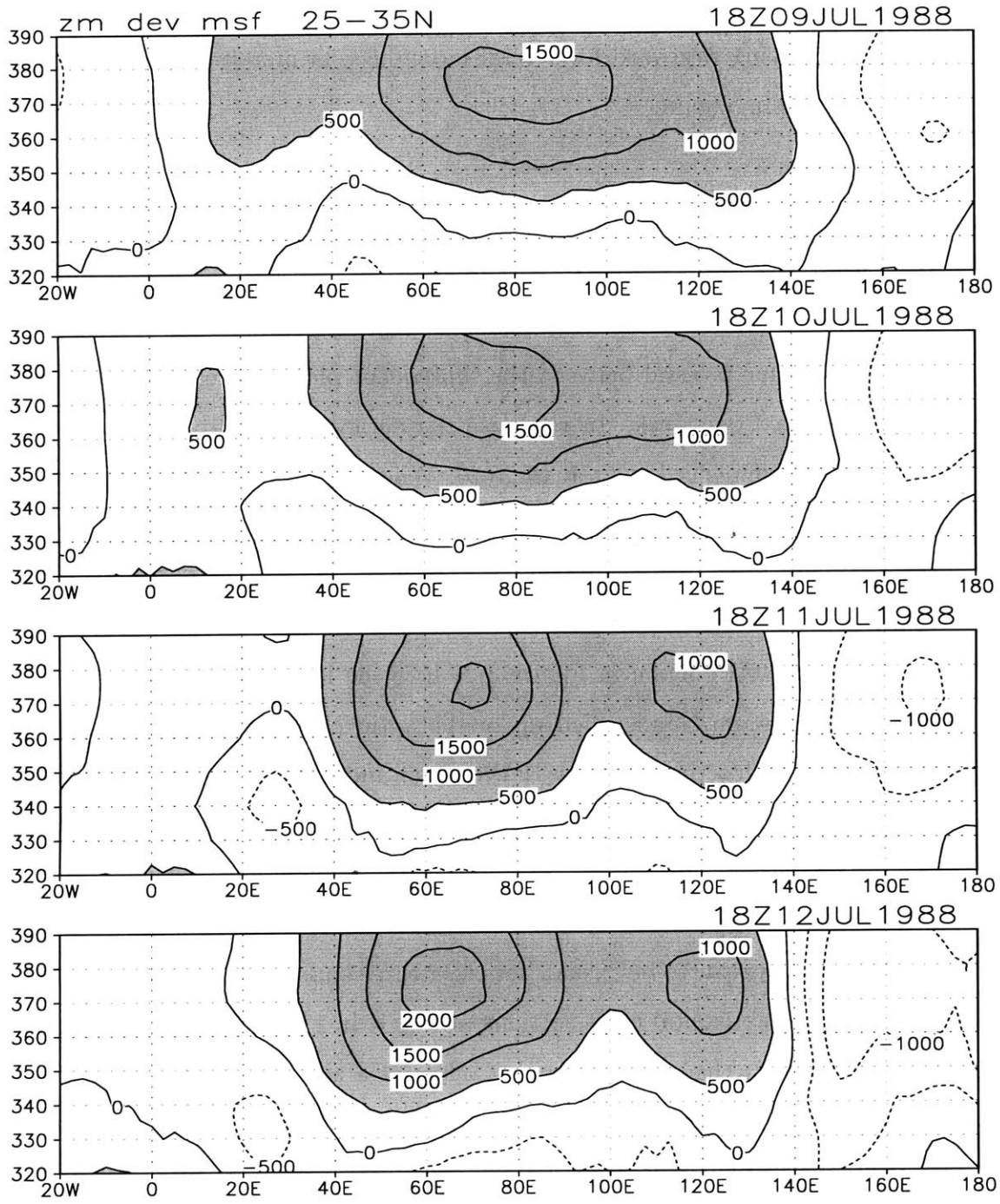

Figure 3-24: Time sequence of vertical cross sections of the perturbation from the zonal mean of M, latitudinally averaged between 25°N and 35°N, given in successive 24-hour intervals from 18 UTC July 9 to 18 UTC July 12, 1988. The values greater than 500 $m^2\ s^{-2}$ are shaded.

event is shown in Figures 3-25 and 3-26. After July 28 at 18 UTC (last plot shown in Figure 3-25), the daughter vortex was recaptured by the mother vortex. This re-unified vortex continued its life, moving westward for several more days, at first strengthening for a short time and then weakening again.

3.3.3 July 1989

July 1989 began with an eddy shedding event. Namely, the end of June was marked with a weak and eccentric anticyclone that was followed by the eddy shedding depicted in Figures 3-27 and 3-28. The time interval between the subsequent plots in these figures is two days. The whole event lasted one week. In this case the anticyclone was centered around 80°E before the shedding commenced (plot at the top). When the shedding happened the mother vortex remained on the eastern side with its center as far east as 100°E, while the daughter vortex detached on the western side and moved northwestward with its center reaching 40°E. This was clearly seen in both fields (vertical cross sections of M in Figure 3-28 also clearly show the shedding). Notice again in Figure 3-27 how the low IPV filament extended from the mother vortex westward and rolled up in the anticyclonic sense (third plot) to form the daughter vortex. This time the low IPV centers and high M were very well spatially correlated (except for the third localized low IPV center which appeared around 75°E and 20°N).

The evolution of both IPV and M fields continued in a somewhat unusual way throughout July (at least for what we saw to be "usual" for other three analyzed years). This is illustrated with the four plots of horizontal cross sections at 370 K in Figure 3-29. After regaining its unified shape by July 7, the anticyclone also achieved a shape such that its western part became stronger and wider in meridional direction (M field), extending more to the north than the eastern part. This whole system was moving westward with time. At the same time lowest values of IPV remained in the eastern part. This whole time period is illustrated by the first plot in Figure 3-29, which shows the fields at 18 UTC, July 11. On July 14, a secondary vortex built up on the east side (centered at 90°E). Two anticyclonic centers continued their lifetime together for ten days. In the first part of this period, two cells were almost of the same strength in both fields (second plot at 18 UTC, July 16). In the later part

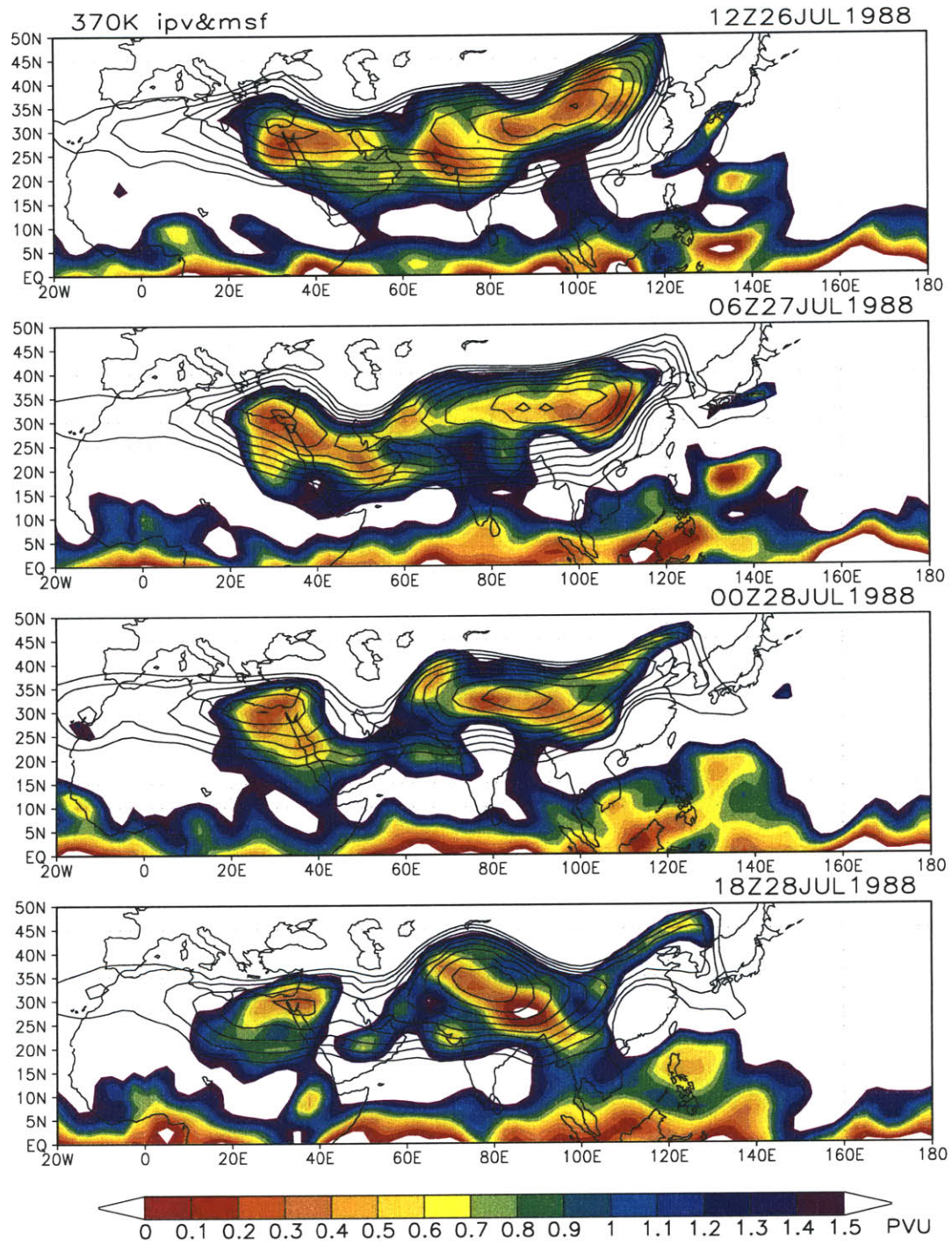

Figure 3-25: Time sequence of IPV (color shading) and M (line contours) fields at 370K given in successive 18-hour intervals from 12 UTC July 26 to 18 UTC July 28, 1988. Minimum value of displayed contour lines is 356500 m^2 s^{-2}. Contour line interval is 250 m^2 s^{-2}.

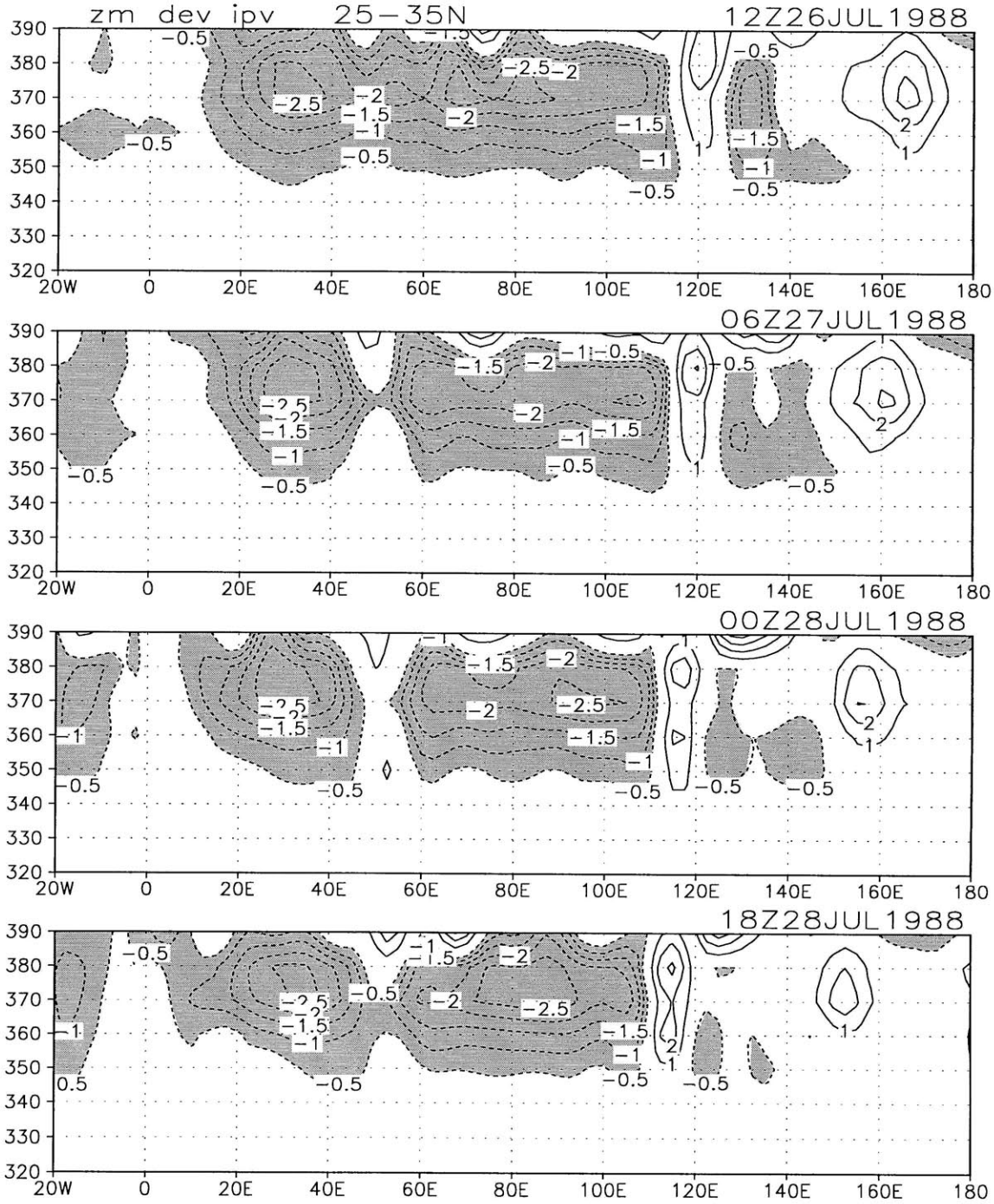

Figure 3-26: Time sequence of vertical cross sections of the perturbation from the zonal mean of IPV, latitudinally averaged between 25°N and 35°N, given in successive 18-hour intervals from 12 UTC July 26 to 18 UTC July 28, 1988. The values smaller than -0.5 PVU are shaded.

of the period, the western cell remained strong in the M field, but the IPV values, although still low (less than 1.5 PVU in the center) were higher than in the eastern cell. The western cell also started to move northward what is shown in third plot at 06 UTC, July 23. Finally, by July 26, the western cell went much northward and weakened, so that only the eastern cell remained to dominate the field. This remaining strong anticyclone (shown in fourth plot at 06 UTC, July 27) moved westward, losing much of its strength by the end of July.

3.3.4 July 1990

The last analyzed year is 1990. We already described the sample case of eddy shedding in July 1990. Before that event the upper tropospheric anticyclone was rather unified with increasing eccentricity in the days preceding our sample case. After the eddy shedding event, the anticyclonic vortex reunited by July 17.

Another shedding event followed in this month (Figures 3-30 and 3-31), starting on July 19 and ending on July 23. In this case, the western cell (daughter vortex) was stronger than the eastern one. It moved slightly northward, but not much westward. After July 21 (bottom plot) it moved back eastward and it was recaptured by the mother vortex again. For the rest of the month the anticyclone remained united.

3.3.5 August

The strong anticyclone usually starts to build up in the first half of June. It is strongest in July and first part of August, and then starts to gradually weaken in the second part of August. Two interesting events in August are presented here. One was the propagation of the whole anticyclone westward in August 1987, and the other one was the shedding event in late August 1988 (starting on August 25, Figure 3-32). Preceding the shedding, the anticyclone was again strong and elongated. When the shedding started and as the western cell was moving westward, the whole system weakened and by the end of August, daughter vortex ceased to exist.

In August 1987 (similar to the case in July 1989) there was a ten day period when the anticyclone moved westward with its center moving from $\sim 90°$E on August 6 to $\sim 50°$E on

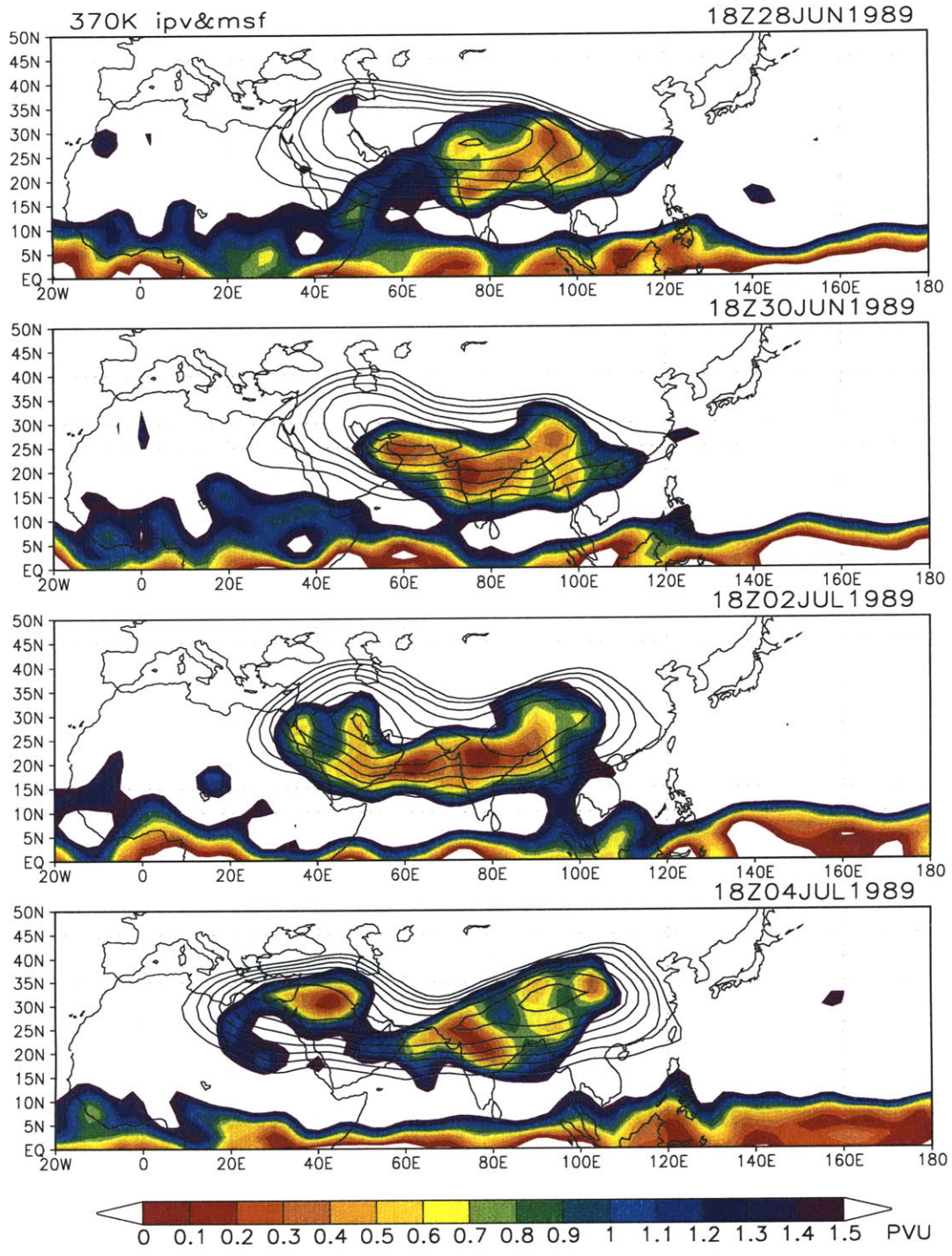

Figure 3-27: Time sequence of IPV (color shading) and M (line contours) fields at 370K given in successive 48-hour intervals from 18 UTC June 28 to 18 UTC July 4, 1989. Minimum value of displayed contour lines is 356000 m^2 s^{-2}. Contour line interval is 250 m^2 s^{-2}.

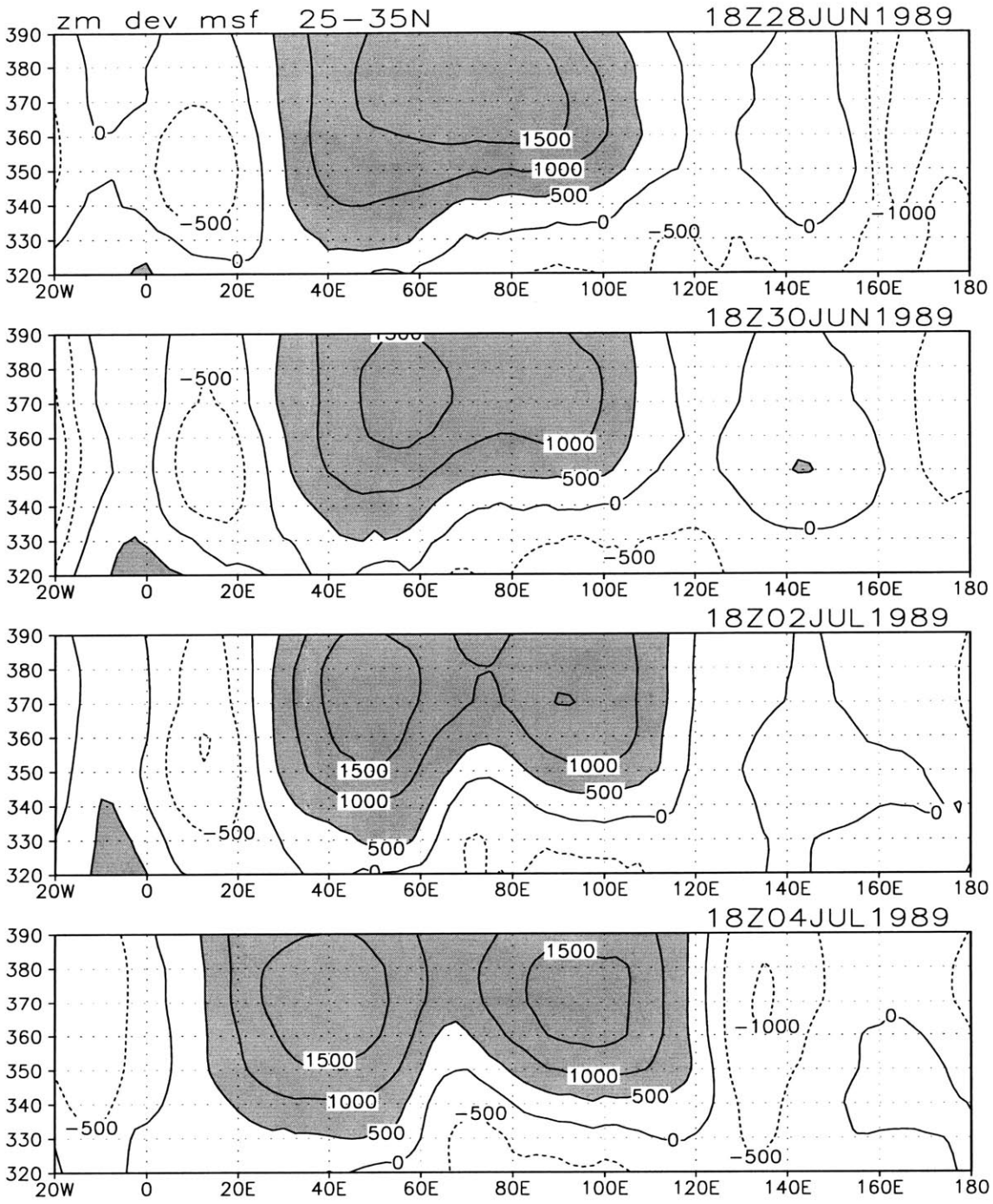

Figure 3-28: Time sequence of vertical cross sections of the perturbation from the zonal mean of M, latitudinally averaged between 25°N and 35°N, given in successive 48-hour intervals from 18 UTC June 28 to 18 UTC July 4, 1989. The values greater than 500 m^2 s^{-2} are shaded.

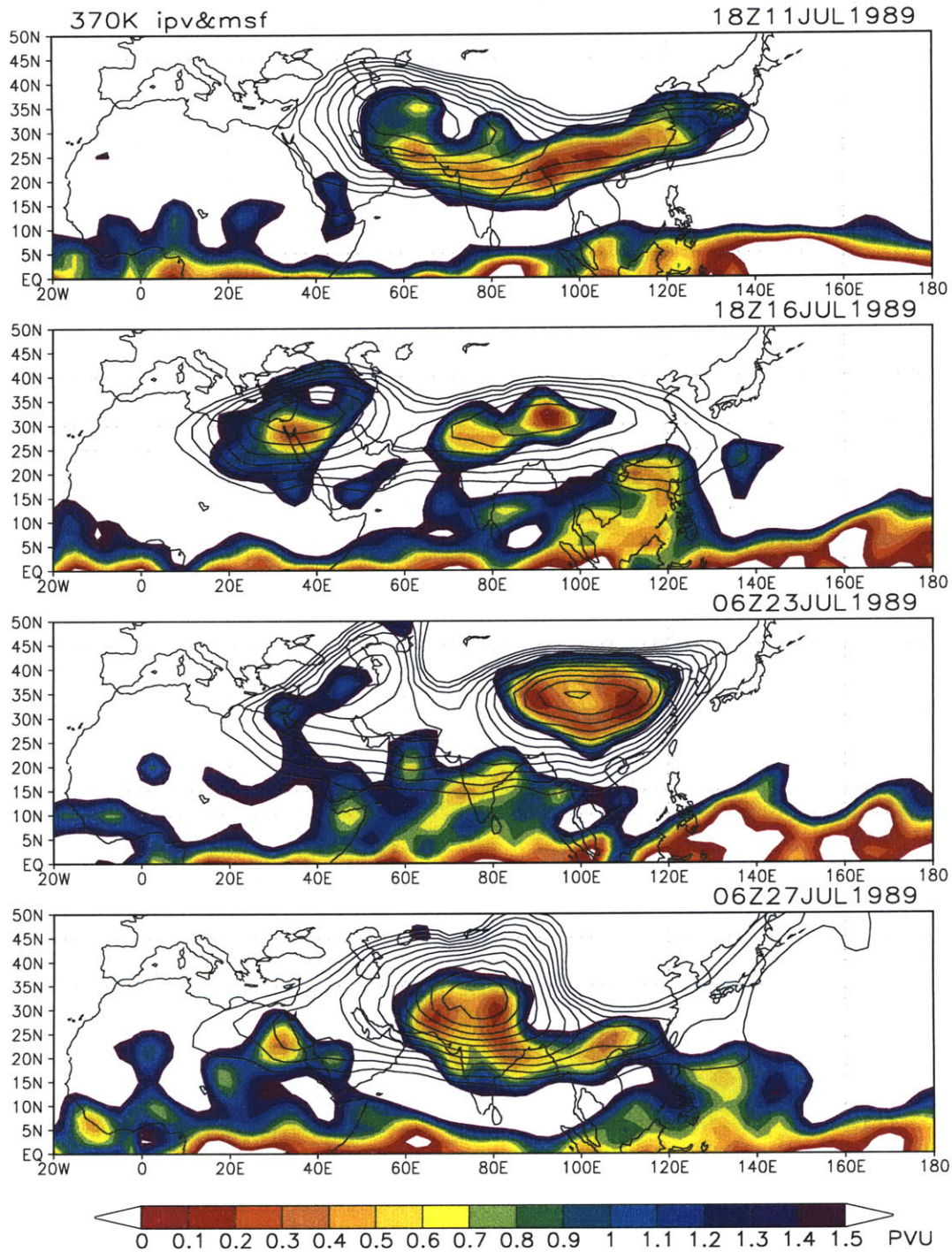

Figure 3-29: IPV (color shading) and M (line contours) fields at 370 K given at 18 UTC July 11, 1988 (first plot), 18 UTC July 16, 1988 (second plot), 06 UTC, July 23, 1988 (third plot), and 06 UTC, July 27, 1988 (fourth plot). Minimum value of displayed contour lines is 356000 m^2 s^{-2}. Contour line interval is 250 m^2 s^{-2}.

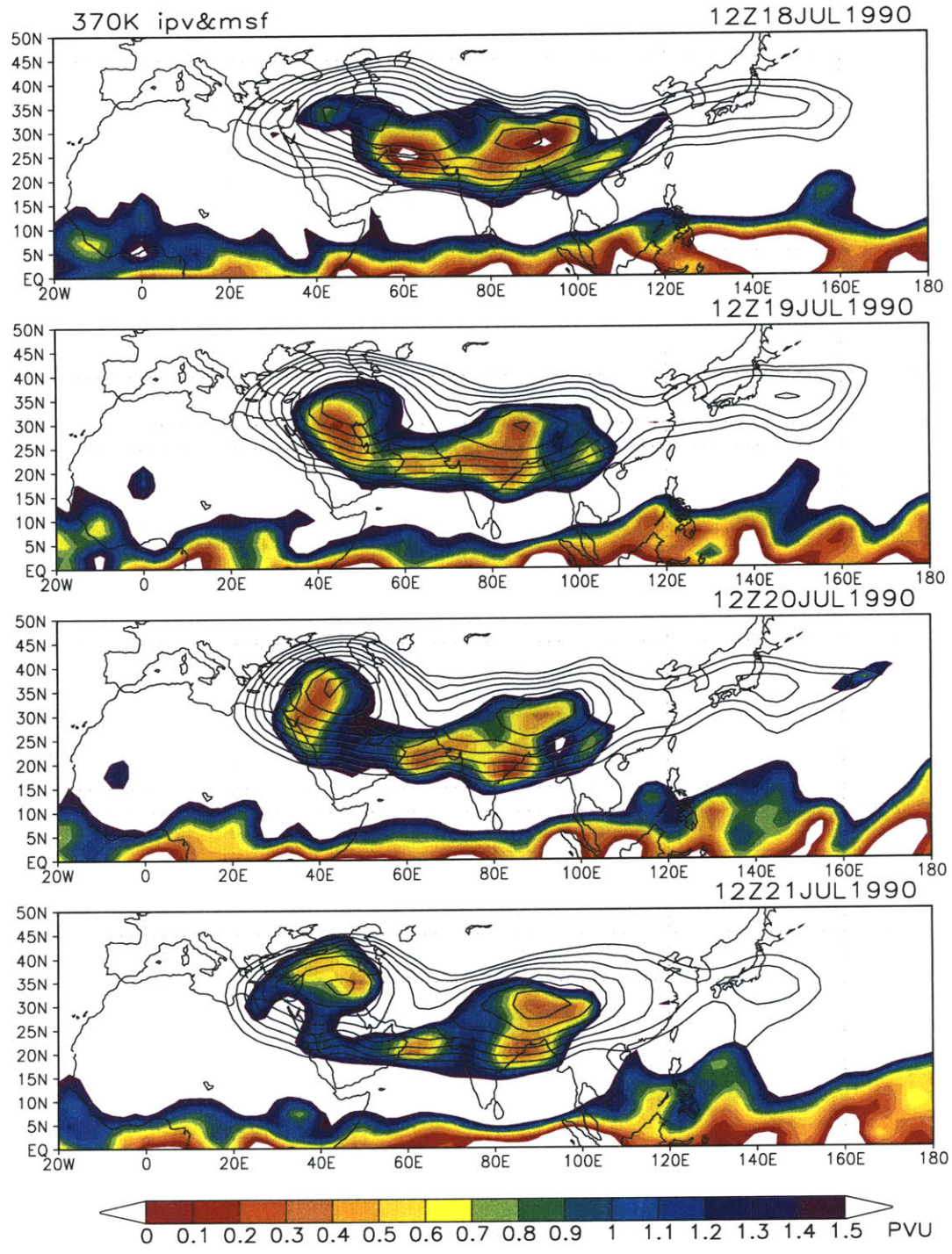

Figure 3-30: Time sequence of IPV (color shading) and M (line contours) fields at 370 K given in successive 24-hour intervals from 12 UTC July 18 to 12 UTC July 21, 1990. Minimum value of displayed contour lines is 356000 m^2 s^{-2}. Contour line interval is 250 m^2 s^{-2}.

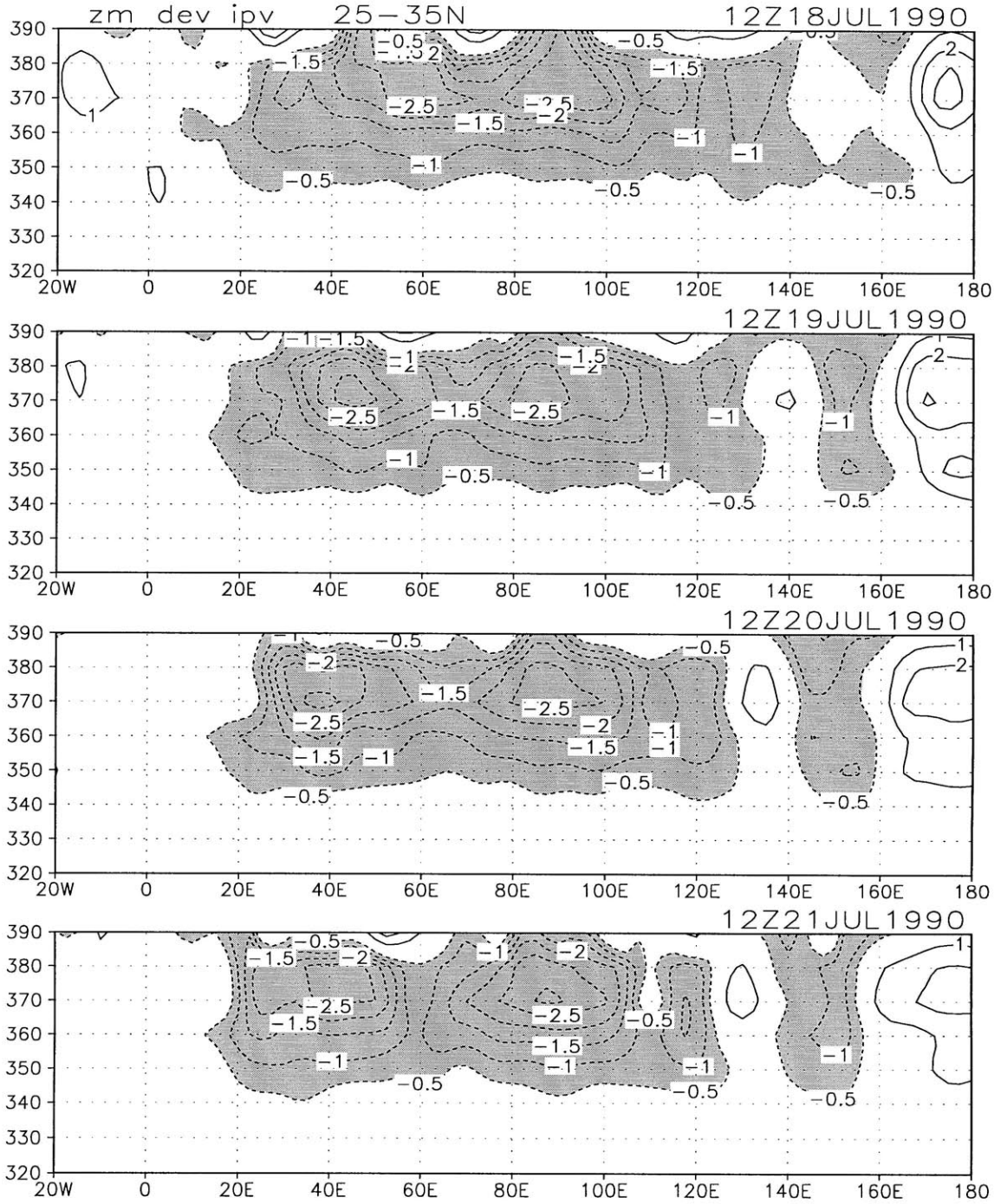

Figure 3-31: Time sequence of vertical cross sections of the perturbation from the zonal mean of IPV, latitudinally averaged between 25°N and 35°N, given in successive 24-hour intervals from 12 UTC July 18 to 12 UTC July 21, 1990. The values smaller than -0.5 PVU are shaded.

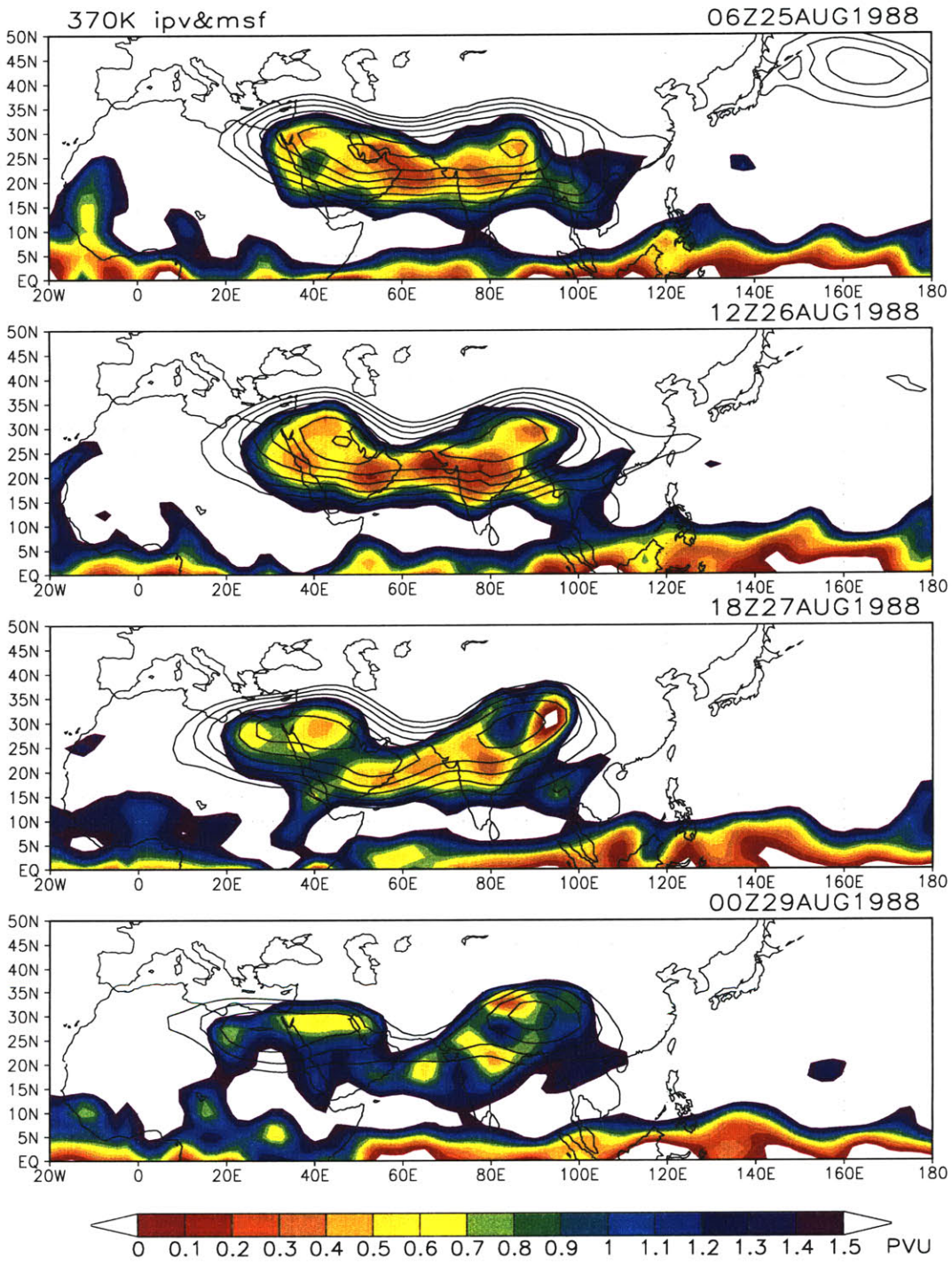

Figure 3-32: Time sequence of IPV (color shading) and M (line contours) fields at 370 K given in successive 30-hour intervals from 06 UTC August 25 to 00 UTC August 29, 1988. Minimum value of displayed contour lines is 356000 m^2 s^{-2}. Contour line interval is 250 $m^2 s^{-2}$.

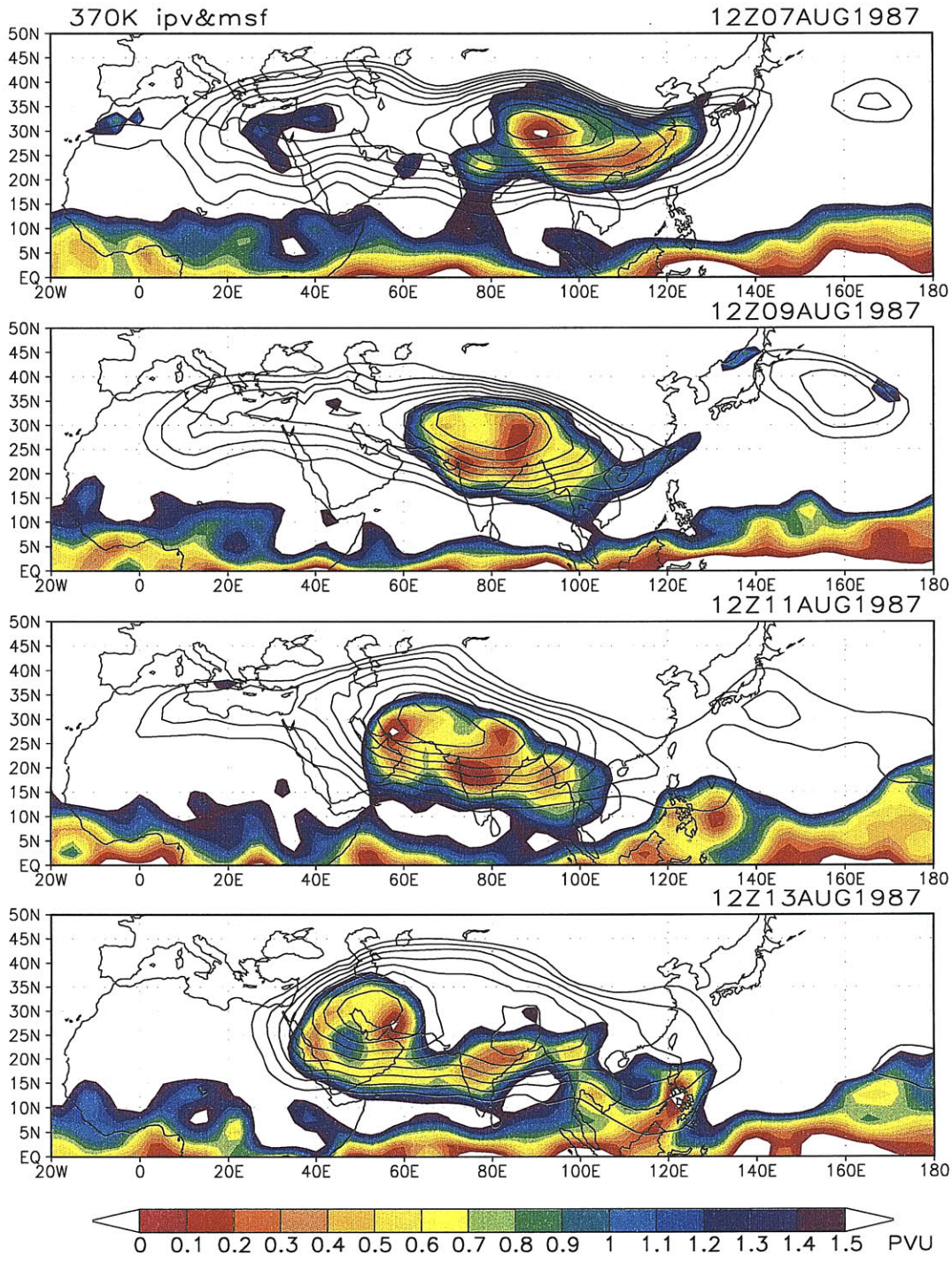

Figure 3-33: Time sequence of IPV (color shading) and M (line contours) fields at 370 K given in successive 48-hour intervals from 12 UTC August 7 to 12 UTC August 13, 1987. Minimum value of displayed contour lines is 356000 m^2 s^{-2}. Contour line interval is 250 $m^2 s^{-2}$.

August 16 (Figure 3-33). The low values of IPV were confined to the area of the maximum values of the streamfunction.

3.4 Relation to the lower levels

The source of the persistent divergent circulation in the upper troposphere is diabatic heating (in the form of latent heating associated with strong convection, and sensible heating from the Tibetan plateau). We noticed that when the shedding happens, the daughter vortex propagates westward (except in the case of July 1988). While it moves away from the source of the diabatic heating, it weakens and finally vanishes.

The establishment of a quantitative relation between the diabatic heating and the state of the upper tropospheric anticyclone would require involved analysis of each individual case. In order to address this question without going into too much detail, we looked at the geopotential height field in the lower levels. We noticed a few interesting connections.

In the lower levels, the cyclonic systems are characterized by smaller scales than the anticyclonic systems above. For example, the monsoon trough extends for $\sim 20°$ in the zonal direction and $\sim 10°$ in the meridional direction. Also, the monsoon depressions that form in the Bay of Bengal and move westward over Indian subcontinent have a horizontal scale of 10-20°. The low which is often seen over Pakistan is about that size as well. All these smaller scale systems contribute to the large area of low pressure between 30°E and 120°E and from Equator to 35°N.

In general, as the cyclonic systems intensifies, the upper level divergent system builds up. The movement of the monsoon depressions and cyclonic systems embedded in the monsoon trough are often accompanied by the movement of the upper tropospheric anticyclonic cells. However, our analysis does not allow us to draw definite conclusions regarding the relationship of the lower level cyclonic systems and the upper level divergent flow. The well-defined trough with one or two cyclonic cells embedded in it is found in cases of shedding as well as when the anticyclone is united. Similarly, the monsoon depressions are found in both cases, too. Still, there were some examples of a clear relation in the development of the lower and upper level systems.

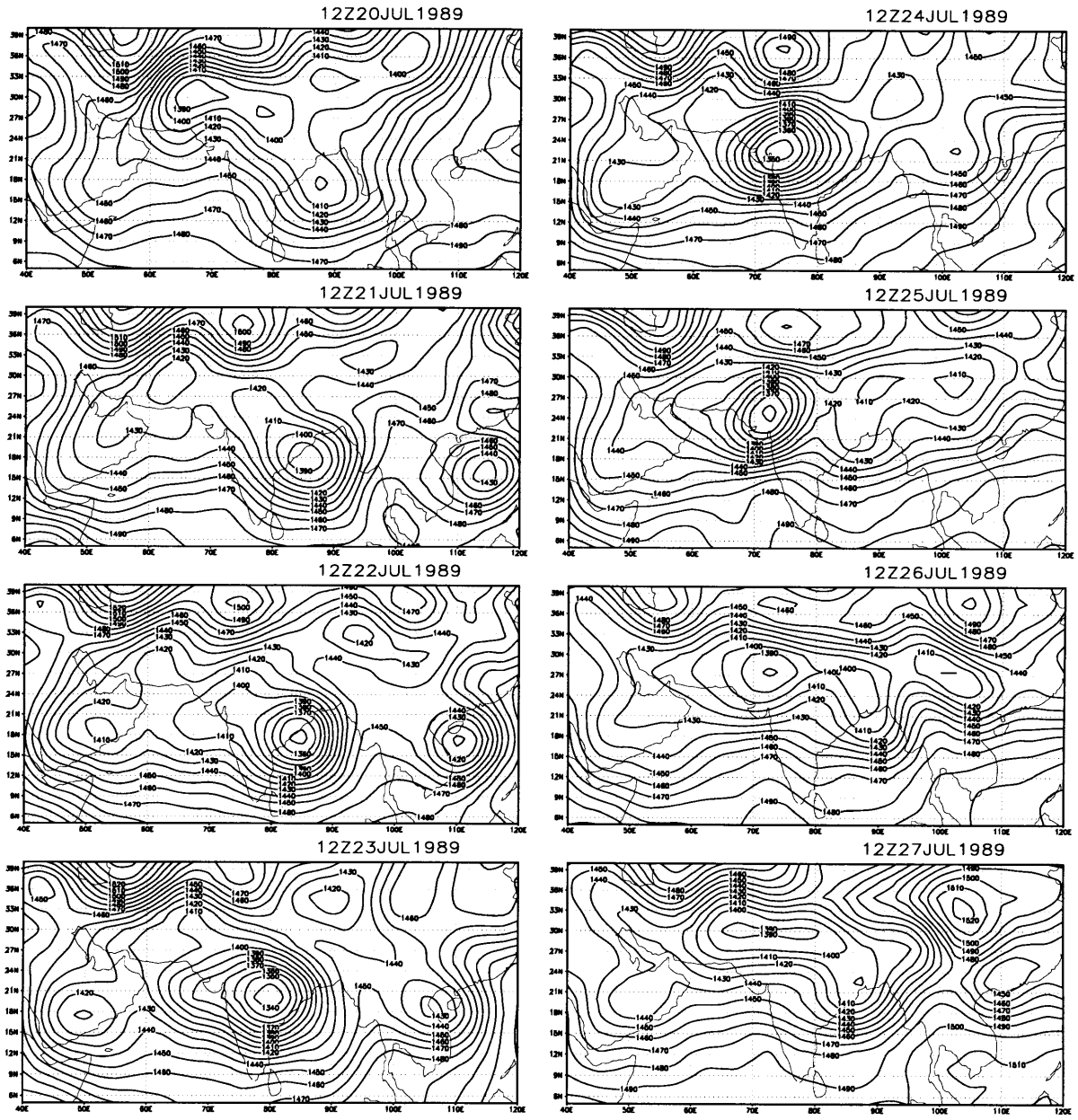

Figure 3-34: Time sequence of geopotential height at 850 mb given in successive 24-hour intervals from 12 UTC July 20 to 12 UTC July 27, 1989. Contour line interval is 10 m.

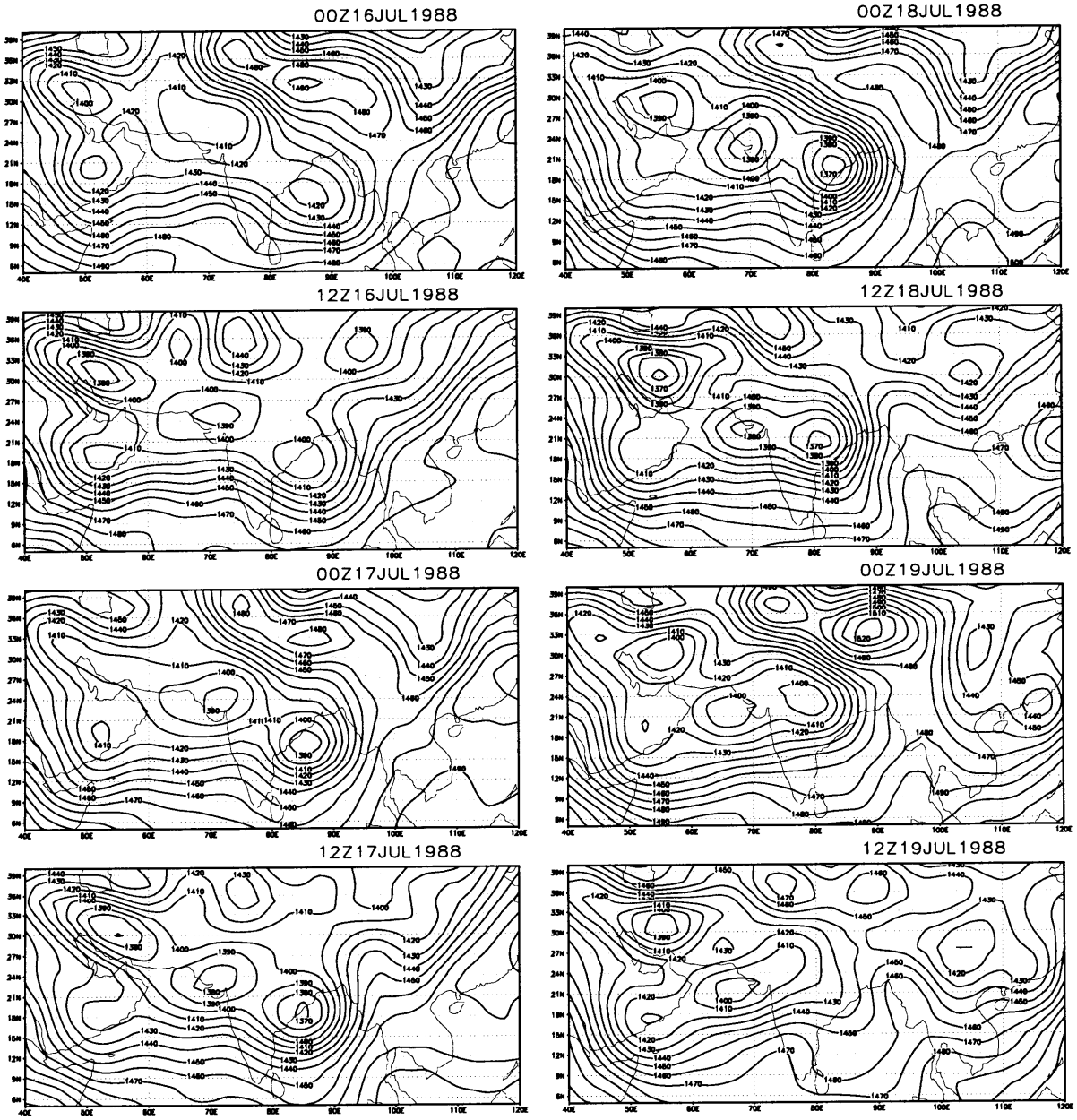

Figure 3-35: Time sequence of geopotential height at 850 mb given in successive 12-hour intervals from 00 UTC July 16 to 12 UTC July 19, 1988. Contour line interval is 10 m.

One example of the clear mutual relation on the large scale between the lower and upper level systems was the case of a strong depression i.e. cyclonic storm, in July 1989. This cyclonic storm formed in the Bay of Bengal (July 20) and then moved northwestward into the continent, with its center reaching 75E°, 28°N (Figure 3-34). This cyclonic storm was formed at a time when the eastern anticyclonic cell became dominant in the upper tropospheric field (Figure 3-29, last two plots), and started to move westward, too.

A somewhat opposite example was a monsoon depression in July 1988. This depression lasted for four days, from July 16 to July 19 (Figure 3-35). This four-day period was a part of the longer ten days period in which the elongated and strong anticyclone was found in the upper troposphere. The depression was moving westward, but the anticyclone above remained in the same position and in the same form. On the other hand, the depression itself may have helped maintain the strong and united character of the anticyclone. This case is also exceptional because the shedding did not occur just two or three days after the formation of the elongated and strong anticyclone (which is usually the case), but rather after the anticyclone persisted for ten days in that state.

In summary, the relationship between lower and upper levels is usually strong, but eddy shedding does not always have an obvious connection to the lower levels.

32), June 28, 1989 (Figures 3-27 and 3-28), July 10, 1990 (Figures 3-9 to 3-14), and July 18, 1990 (Figures 3-30 and 3-31). In the event that started on July 5, 1987 (Figures 3-19 and 3-20), the western cell did not move westward. In the eddy shedding event in July 1988 (Figures 3-23 and 3-24) the daughter cell was shed on the eastern side. In all cases of shedding we found the daughter vortex to be smaller but still of comparable dimensions to the mother vortex. The whole system of two anticyclones has a size equal or larger than initial monsoonal anticyclone (spreading over about 100° longitude and 30° latitude). The shedding appears to be rather shallow, mainly confined between 300 and 100 mb. The relationship between lower and upper levels is addressed here but it is not studied in a great detail. We did not find a unique pattern in the behavior in the lower levels when eddy shedding occurs in the upper troposphere. A detailed analysis for each case would probably give more definite conclusions.

Chapter 4

Conclusion

The upper tropospheric divergent flow in the area of the Asian summer monsoon is present during the whole summer, but it varies greatly in form and strength. The most dramatic changes are seen during eddy shedding events, and during the westward propagation of the anticyclone.

Eddy shedding seems to be a regular phenomenon. It is found every summer (at least in the 1987-1990 data studied here as well as in year 1996 not discussed here). We do not find periodicity in its occurrence. The duration of the shedding varies but it is usually four to eight days. In most cases when the anticyclone strengthens and elongates the shedding happens after two or three days.

Synoptic conditions just prior to eddy shedding were quite compatible with those in the model of Hsu (1998) and Hsu and Plumb (1998). Both in the modeled flow and in the atmosphere, when the strip of low PV embedded in the high PV surrounding becomes rather narrow and long enough in zonal direction, it becomes unstable and sheds eddies. Namely, in the quite elongated eddy, flow is close to parallel and the flow is dynamically unstable due to the change of sign in PV gradient. However, the atmosphere as a complex system often exhibits different behavior from the ideal modeled cases.

In the four analyzed years we found eight cases of eddy shedding. In almost all of these cases, the daughter cell was shed on the western side. The usual evolution after the shedding starts is the westward propagation of the daughter cell. These events started in July 25, 1987 (Figures 3-21 and 3-22), July 26, 1988 (Figures 3-25 and 3-26), August 25, 1988 (Figure 3-

Bibliography

Andrews, D. G., J. R. Holton, and C. B. Leovy, 1987: *Middle Atmosphere Dynamics.* Academic Press, Inc. pp 489.

Das, P. K., 1987: Short- and long-range monsoon prediction in India, in *Monsoons.* Wiley-Interscience Publication, 549-578.

Desai, D. S., 1987: Field of vorticity, divergence, and vertical velocity associated with break and strong monsoon, *Mausam*, **38**, 419-424.

Held, I. M. and A. Y. Hou, 1980: Nonlinear axially symmetric circulations in a nearly inviscid atmosphere, *J. Atmos. Sci.*, **37**, 515-533.

Hoskins, B. J., M. F. McIntyre, and A. W. Robertson, 1985: On the use and significance of isentropic potential vorticity maps, *Quart. J. R. Met. Soc.*, **111**, 877-946.

Hoskins, B. J., and M. J. Rodwell, 1995: A model of the Asian summer monsoon. Part I: The global scale, *J. Atmos. Sci.*, **52**, 1329-1340.

Hsu, C. J., 1998: Eddy shedding from nonaxisymmetric, divergent anticyclones with application to the Asian monsoon anticyclone. MIT Ph.D. thesis, 130 pp.

Hsu, C. J. and R. A. Plumb, 1998: Non-axisymmetric thermally driven circulations and upper tropospheric monsoon dynamics, to be published in *J. Atmos. Sci.*

Inoue, T., 1997: Contrast of 87/88 Indian summer monsoon observed by split window measurements, *Adv. Space Res.*, **19**, 447-455.

Kalnay, E., M. Kanamitsu, R. Kistler, W. Collins, D. Deaven, L. Gandin, M. Iredell, S. Saha, G. White, J. Woollen, Y. Zhu, M. Chelliah, W. Ebisuzaki, W. Higgins, J. Janowiak, K. C. Mo, C. Ropelewski, J. Wang, A. Leetmaa, R. Reynolds, Roy Jenne, Dennis Joseph, 1996: The NCEP/NCAR 40-year reanalysis project, *Bull. Amer. Meteor. Soc.*, **77**, 437-471.

Krishnamurti, T. N., H. S. Bedi, and M. Subramaniam, 1989: The summer monsoon of 1987, *J. Climate*, **2**, 321-340.

Krishnamurti, T. N., H. S. Bedi, and M. Subramaniam, 1990: The summer monsoon of 1988, *Meteor. Atmos. Physics*, **42**, 19-37.

Lau, K.-H., and N.-C. Lau, 1990: Observed structure and propagation characteristics of tropical summertime synoptic scale disturbances, *Mon. Wea. Rev.*, **118**, 1888-1913.

Lindzen, S. R. and A. Y. Hou, 1988: Hadley circulation for zonally averaged heating centered off the equator, *J. Atmos. Sci.*, **45**, 2416-2427.

Sardeshmukh, P. D., and I. M. Held, 1984: The vorticity balance in the tropical upper troposphere of a general circulation model, *J. Atmos. Sci.*, **41**, 768-778.

Sardeshmukh, P. D., and B. J. Hoskins, 1985: Vorticity balance in the tropics during the 1982-83 El Nino-Southern Oscillation event, *Quart. J. R. Met. Soc.*, **111**, 261-278.

Schaack, T K., and D. R. Johnson, 1994: January and July global distributions of atmospheric heating for 1986, 1987, and 1988, *J. Climate*, **7**, 1270-1285.

Slingo, J., 1997, The Indian summer monsoon and its variability, to appear in *Beyond El Nino: Decadal Variability in the Climate System*, Springer.

Yanai, M. and T. Tomita, 1998: Seasonal and interannual variability of atmospheric heat sources and moisture sinks as determined from NCEP-NCAR reanalysis, *J. Climate*, **11**, 463-482.